
Landscape Analysis for Surrogate Models in the Evolutionary Black-Box Context

Zbyněk Pitra

z.pitra@gmail.com

Faculty of Nuclear Sciences and Physical Engineering, Czech Technical University
Břehová 7, 115 19 Prague, Czech Republic

Jan Koza

koza@cs.cas.cz

Faculty of Information Technology, CTU in Prague,
Thákurova 9, 160 00 Prague 6, Czech Republic

Jiří Tumpach

tumpach@cs.cas.cz

Faculty of Mathematics and Physics, Charles University in Prague,
Malostran. nám. 25, 118 00 Prague, Czech Republic

Martin Holeňa

martin@cs.cas.cz

Institute of Computer Science, Czech Academy of Sciences,
Pod Vodárenskou věží 2, 182 07 Prague, Czech Republic

Abstract

Surrogate modeling has become a valuable technique for black-box optimization tasks with expensive evaluation of the objective function. In this paper, we investigate the relationship between the predictive accuracy of surrogate models and features of the black-box function landscape. We also study properties of features for landscape analysis in the context of different transformations and ways of selecting the input data. We perform the landscape analysis of a large set of data generated using runs of a surrogate-assisted version of the Covariance Matrix Adaptation Evolution Strategy on the noiseless part of the Comparing Continuous Optimisers benchmark function testbed.

Keywords

Black-box optimization, Surrogate modeling, Landscape analysis, Metalearning CMA-ES

1 Introduction

When solving a real-world optimization problem we often have no information about the analytic form of the objective function. Evaluation of such *black-box functions* is frequently expensive in terms of time and money (Baerns and Holeňa, 2009; Lee et al., 2016; Zaefferer et al., 2016), which has been for two decades the driving force of research into *surrogate modeling* of black-box objective functions (Büche et al., 2005; Forrester and Keane, 2009; Jin, 2011). Given a set of observations, a surrogate model can be fitted to approximate the landscape of the black-box function.

The *Covariance Matrix Adaptation Evolution Strategy* (CMA-ES) by Hansen (2006), which we consider the state-of-the-art evolutionary black-box optimizer, has been frequently combined with surrogate models. However, different surrogate models can show significant differences in the performance of the same optimizer on different

data (Pitra et al., 2021). Such performance can also change during the algorithm run due to varying landscape of the black-box function in different parts of the search space. Moreover, the predictive accuracy of individual models is strongly influenced by the choice of their parameters. Therefore, the investigation of the relationships between the settings of individual models and the optimized data is necessary for better understanding of the whole surrogate modeling task.

In last few years, research into landscape analysis of objective functions (cf. the overview by Kerschke (2017)) has emerged in the context of algorithm selection and algorithm configuration. However, to our knowledge, such features have been investigated in connection with surrogate models in the context of black-box optimization using static settings only, where the model is selected once at the beginning of the optimization process (Saini et al., 2019). Moreover, the analysis of landscape features also had less attention so far than it deserves and not in the context of surrogate models (Renau et al., 2019, 2020).

In this paper, we study properties of features representing the fitness landscape in the context of the data from actual runs of a surrogate-assisted version of the CMA-ES on the noiseless part of the Comparing Continuous Optimisers (COCO) benchmark function testbed (Hansen et al., 2016). From the large number of available features, we select a small number of representatives for subsequent research, based on their robustness to sampling and similarity to other features. Basic investigation in connection with landscape features of CMA-ES assisted by a surrogate model based on Gaussian processes (Rasmussen and Williams, 2006) was recently presented in a conference paper by Pitra et al. (2019). Here, we substantially more thoroughly investigate the relationships between selected representatives of landscape features and the error of several kinds of surrogate models using different settings of their parameters and the criteria for selecting points for their training. Such study is crucial due to completely different properties of data from runs of a surrogate-assisted algorithm compared with generally utilized sampling strategies, which imply different values of landscape features as emphasized in Renau et al. (2020).

The paper is structured as follows. Section 2 briefly summarizes the basics of surrogate modeling in the context of the CMA-ES, surrogate models used in this investigation, and landscape features from the literature. In Section 3, properties of landscape features are thoroughly tested and their connection to surrogate models is analysed. Section 4 concludes the paper and suggests a few future research objectives.

2 Background

The goal of *black-box* optimization is to find a point For this function, we are only able to obtain the value $\mathbb{f}(\mathbf{x})$ of an *objective function* \mathbb{f} , a. k. a. *fitness*, in a point \mathbf{x} , but no analytic expression is known, neither an explicit one as a composition of known mathematical functions, nor an implicit one as a solution of an equation (e. g., algebraic or differential). In case of minimization:

$$\mathbf{x}^* = \arg \min_{\mathbf{x} \in \mathcal{S}} \mathbb{f}(\mathbf{x}). \quad (1)$$

2.1 Surrogate Modeling in the Context of the CMA-ES

Black-box optimization problems frequently appear in the real world, where the values of a fitness function $\mathbb{f}(\mathbf{x})$ can be obtained only empirically through experiments or via computer simulations. As recalled in the Introduction, such empirical evaluation is sometimes very time-consuming or expensive. Thus, we assume that evaluating the fitness represents a considerably higher cost than training a regression model.

Algorithm 1 Pseudocode of the CMA-ES

Input: λ (population-size), \mathfrak{fb} (original fitness function), $(w_i)_{i=1}^\mu$, μ_w (selection and recombination parameters), c_σ , d_σ (step-size control parameters), c_c , c_I , c_μ (covariance matrix adaptation parameters)

- 1: **init** $g = 0$, $\sigma^{(0)} > 0$, $\mathbf{m}^{(0)} \in \mathbb{R}^D$, $\mathbf{C}^{(0)} = \mathbf{I}$, $\mathbf{p}_\sigma^{(0)} = \mathbf{0}$, $\mathbf{p}_c^{(0)} = \mathbf{0}$, $\mu = \lfloor \lambda/2 \rfloor$
 - 2: **repeat**
 - 3: $\mathbf{x}_k \leftarrow \mathbf{m}^{(g)} + \sigma^{(g)} \mathcal{N}(\mathbf{0}, \mathbf{C}^{(g)}) \quad k = 1, \dots, \lambda$
 - 4: $\mathfrak{fb}_k \leftarrow \mathfrak{fb}(\mathbf{x}_k) \quad k = 1, \dots, \lambda$
 - 5: $\mathbf{m}^{(g+1)} \leftarrow \sum_{i=1}^\mu w_i \mathbf{x}_{i:\lambda}$, where $\mathbf{x}_{i:\lambda}$ is the i -th best individual out of $\mathbf{x}_1, \dots, \mathbf{x}_\lambda$
 - 6: $\mathbf{p}_\sigma^{(g+1)} \leftarrow (1 - c_\sigma) \mathbf{p}_\sigma^{(g)} + \sqrt{c_\sigma(2 - c_\sigma)\mu_w} \mathbf{C}^{(g)^{-1/2}} \frac{\mathbf{m}^{(g+1)} - \mathbf{m}^{(g)}}{\sigma^{(g)}}$
 - 7: $h_\sigma \leftarrow \mathbb{I} \left(\|\mathbf{p}_\sigma^{(g+1)}\| < \sqrt{1 - (1 - c_\sigma)^{2(g+1)}} \left(1.4 + \frac{2}{D+1} \right) \mathbb{E} \|\mathcal{N}(0, 1)\| \right)$
 - 8: $\mathbf{p}_c^{(g+1)} \leftarrow (1 - c_c) \mathbf{p}_c^{(g)} + h_\sigma \sqrt{c_c(2 - c_c)\mu_w} \frac{\mathbf{m}^{(g+1)} - \mathbf{m}^{(g)}}{\sigma^{(g)}}$
 - 9: $\mathbf{C}_\mu \leftarrow \sum_{i=1}^\mu w_i \sigma^{(g)^{-2}} (\mathbf{x}_{i:\lambda}^{(g+1)} - \mathbf{m}^{(g)}) (\mathbf{x}_{i:\lambda}^{(g+1)} - \mathbf{m}^{(g)})^\top$
 - 10: $\mathbf{C}^{(g+1)} \leftarrow (1 - c_I - c_\mu) \mathbf{C}^{(g)} + c_I \mathbf{p}_c^{(g+1)} \mathbf{p}_c^{(g+1)\top} + c_\mu \mathbf{C}_\mu$
 - 11: $\sigma^{(g+1)} \leftarrow \sigma^{(g)} \exp \left(\frac{c_\sigma}{d_\sigma} \left(\frac{\|\mathbf{p}_\sigma^{(g+1)}\|}{\mathbb{E} \|\mathcal{N}(0, \mathbf{I})\|} - 1 \right) \right)$
 - 12: $g \leftarrow g + 1$
 - 13: **until** stopping criterion is met
- Output:** \mathbf{x}_{res} (resulting optimum)

As a *surrogate model*, we understand any regression model $\widehat{\mathfrak{fb}} : \mathcal{X} \rightarrow \mathbb{R}$ that is trained on the already available input-output value pairs stored in an *archive* $\mathcal{A} = \{(\mathbf{x}_i, y_i) \mid y_i = \mathfrak{fb}(\mathbf{x}_i), i = 1, \dots, N\}$, and is used instead of the original expensive fitness to evaluate some of the points needed by the optimization algorithm.

2.1.1 The CMA-ES

The *Covariance Matrix Adaptation Evolution Strategy* (CMA-ES) proposed by Hansen and Ostermeier (1996) has become one of the most successful algorithms in the field of continuous black-box optimization. Its pseudocode is outlined in Algorithm 1.

After generating λ new candidate solutions using the mean $\mathbf{m}^{(g)}$ of the mutation distribution added to a random Gaussian mutation with covariance matrix $\mathbf{C}^{(g)}$ in generation g (step 3), the fitness function \mathfrak{fb} is evaluated for the new offspring (step 4). The new mean $\mathbf{m}^{(g+1)}$ of the mutation distribution is computed as the weighted sum of the μ best points among the λ ordered offspring $\mathbf{x}_1, \dots, \mathbf{x}_\lambda$ (step 5).

The sum of consecutive successful mutation steps of the algorithm in the search space $(\mathbf{m}^{(g+1)} - \mathbf{m}^{(g)})/\sigma^{(g)}$ is utilized to compute two *evolution path* vectors \mathbf{p}_σ and \mathbf{p}_c (step 6). Successful steps are tracked in the sampling space and stored in \mathbf{p}_σ using the transformation $\mathbf{C}^{(g)^{-1/2}}$. The evolution path \mathbf{p}_c is calculated similarly to \mathbf{p}_σ ; however, the coordinate system is not changed (step 8). The two remaining evolution path elements are a decay factor c_σ decreasing the impact of successful steps with increasing generations, and μ_w used to normalize the variance of \mathbf{p}_σ .

The covariance matrix adaptation (step 10) is performed using *rank-one* and *rank- μ* updates. The rank-one update utilizes \mathbf{p}_c to calculate the covariance matrix $\mathbf{p}_c \mathbf{p}_c^\top$. The rank- μ update cumulates successful steps of μ best individuals in matrix \mathbf{C}_μ (step 9).

The step-size σ (step 11) is updated according to the ratio between the evolution path length $\|\mathbf{p}_\sigma\|$ and the expected length of a random evolution path. If the ratio is

greater than 1, the step-size is increasing, and decreasing otherwise.

The CMA-ES uses restart strategies to deal with multimodal fitness landscapes and to avoid being trapped in local optima. A multi-start strategy where the population size is doubled in each restart n_r is referred to as IPOP-CMA-ES (Auger and Hansen, 2005).

2.1.2 Training Sets

The level of the model precision is highly determined by the selection of the points from the archive to the training set \mathcal{T} . Considering the surrogate models we use in this paper, we list the following training set selection (TSS) methods:

- ◇ *TSS full*, taking all the already evaluated points, i. e., $\mathcal{T} = \mathcal{A}$,
- ◇ *TSS knn*, selecting the union of the sets of k -nearest neighbors of all points for which the fitness should be predicted, where k is user defined (e. g., in Kern et al. (2006)),
- ◇ *TSS nearest*, selecting the union of the sets of k -nearest neighbors of all points for which the fitness should be predicted, where k is maximal such that the total number of selected points does not exceed a given maximum number of points N_{\max} and no point is further from current mean $\mathbf{m}^{(g)}$ than a given maximal distance r_{\max} (e. g., in Bajer et al. (2019)).

The models in this paper use the Mahalanobis distance given by the CMA-ES matrix $\sigma^2\mathbf{C}$ (see Equation 4) for selecting points into training sets, similarly to, e. g., Kruis-selbrink et al. (2010). Considering the fact that TSS knn is the original TSS method of the model from Kern et al. (2006) only (see Subsection 2.1.3), we list it here and utilize it only in connection with this particular model.

2.1.3 Response Surfaces

Basically, the purpose of surrogate modeling – to approximate an unknown functional dependence – coincides with the purpose of *response surface modeling* in the design of experiments (Hosder et al., 2001; Myers et al., 2009). Therefore, it is not surprising that typical response surface models, i. e., *low order polynomials*, also belong to most traditional and most successful surrogate models (Rasheed et al., 2005; Kern et al., 2006; Auger et al., 2013; Hansen, 2019). Here, we present two surrogate models using at most quadratic polynomial utilized in two successful surrogate-assisted variants of the CMA-ES: the local-metamodel-CMA (lmm-CMA) by Kern et al. (2006) and the linear-quadratic CMA-ES (lq-CMA-ES) by Hansen (2019).

Local-metamodel is a specific full quadratic model $f_j : \mathbb{R}^D \rightarrow \mathbb{R}$ trained for $\mathbf{x}_j, j = 1, \dots, \lambda$ used in the lmm-CMA (Auger et al., 2013),

$$f_j(\mathbf{x}) = (\mathbf{x} - \mathbf{x}_j)^\top \mathbf{A}_j (\mathbf{x} - \mathbf{x}_j) + (\mathbf{x} - \mathbf{x}_j)^\top \mathbf{b}_j + c_j \text{ with } \mathbf{A}_j \in \mathbb{R}^{D \times D}, \mathbf{b}_j \in \mathbb{R}^D, c_j \in \mathbb{R}. \quad (2)$$

The model f_j is trained on the set $N_k(\mathbf{x}_j; \mathcal{A})$ of a given number k of nearest neighbors of \mathbf{x}_j with respect to a given archive \mathcal{A} ,

$$N_k(\mathbf{x}_j; \mathcal{A}) \subset \mathcal{A}, |N_k(\mathbf{x}_j; \mathcal{A})| = k, (\forall \mathbf{x} \in N_k(\mathbf{x}_j; \mathcal{A})) (\forall \mathbf{x}' \in \mathcal{A} \setminus N_k(\mathbf{x}_j; \mathcal{A})) d(\mathbf{x}, \mathbf{x}_j) \leq d(\mathbf{x}', \mathbf{x}_j). \quad (3)$$

As the distance d in (3), the Mahalanobis distance for $\sigma^2\mathbf{C}$ is used:

$$d_{\sigma^2\mathbf{C}}(\mathbf{x}, \mathbf{y}) = \sqrt{(\mathbf{x} - \mathbf{y})^\top \sigma^{-2}\mathbf{C}^{-1}(\mathbf{x} - \mathbf{y})}. \quad (4)$$

The *linear-quadratic model* in the algorithm lq-CMA-ES differs from the lmm-CMA in an important aspect:

Whereas surrogate models in the lmm-CMA are always full quadratic, the lq-CMA-ES admits also pure quadratic or linear models. The employed kind of model depends on the number of points in \mathcal{T} (according to the employed TSS method).

2.1.4 Gaussian Processes

A Gaussian process (GP) is a collection of random variables $(f(\mathbf{x}))_{\mathbf{x} \in \mathcal{X}}$, $\mathcal{X} \subset \mathbb{R}^D$, any finite number of which has a joint Gaussian distribution (Rasmussen and Williams, 2006). The GP is completely defined by a mean function $m : \mathcal{X} \rightarrow \mathbb{R}$, typically assumed to be some constant m_{GP} , and by a covariance function $\kappa : \mathcal{X} \times \mathcal{X} \rightarrow \mathbb{R}$ such that

$$\mathbb{E}f(\mathbf{x}) = m_{\text{GP}}, \quad \text{cov}(f(\mathbf{x}), f(\mathbf{x}')) = \kappa(\mathbf{x}, \mathbf{x}'), \quad \mathbf{x}, \mathbf{x}' \in \mathcal{X}. \quad (5)$$

The value of $f(\mathbf{x})$ is typically a noisy observation $y = f(\mathbf{x}) + \varepsilon$, where ε is a zero-mean Gaussian noise with a variance $\sigma_n^2 > 0$. Then

$$\text{cov}(y, y') = \kappa(\mathbf{x}, \mathbf{x}') + \sigma_n^2 \mathbb{I}(\mathbf{x} = \mathbf{x}'), \quad (6)$$

where $\mathbb{I}(p)$ equals 1 when a proposition p is true and 0 otherwise.

Consider now the prediction of the random variable $f(\mathbf{x}_*)$ in a point $\mathbf{x}_* \in \mathcal{X}$ if we already know $(\mathfrak{bb}(\mathbf{x}_1), \dots, \mathfrak{bb}(\mathbf{x}_n))^\top = (f(\mathbf{x}_1) + \varepsilon_1, \dots, f(\mathbf{x}_n) + \varepsilon_n)^\top$ in points $\mathbf{x}_1, \dots, \mathbf{x}_n$. Introduce the vectors $\mathbf{X} = (\mathbf{x}_1, \dots, \mathbf{x}_n)^\top$, $\mathbf{y} = (\mathfrak{bb}(\mathbf{x}_1), \dots, \mathfrak{bb}(\mathbf{x}_n))^\top$, $\mathbf{k}_* = (\kappa(\mathbf{x}_1, \mathbf{x}_*), \dots, \kappa(\mathbf{x}_n, \mathbf{x}_*))^\top$ and the matrix $\mathbf{K} \in \mathbb{R}^{n \times n}$ such that $(\mathbf{K})_{i,j} = \kappa(\mathbf{x}_i, \mathbf{x}_j)$. Then the probability density of the vector \mathbf{y} is

$$p(\mathbf{y}; m(\mathbf{X}), \kappa, \sigma_n^2) = \frac{\exp\left(-\frac{1}{2}(\mathbf{y} - m_{\text{GP}})^\top \mathbf{K}^{-1}(\mathbf{y} - m_{\text{GP}})\right)}{\sqrt{(2\pi)^D \det(\mathbf{K} + \sigma_n^2 \mathbf{I}_n)}}, \quad (7)$$

where $\det(\mathbf{A})$ denotes the determinant of a matrix \mathbf{A} . Further, as a consequence of the assumption of Gaussian joint distribution, also the conditional distribution of $f(\mathbf{x}_*)$ conditioned on \mathbf{y} is Gaussian:

$$\mathcal{N}(m(\mathbf{x}_*) + \mathbf{k}_* \mathbf{K}^{-1}(\mathbf{y} - m_{\text{GP}}), \kappa(\mathbf{x}_*, \mathbf{x}_*) - \mathbf{k}_*^\top \mathbf{K}^{-1} \mathbf{k}_*). \quad (8)$$

2.1.5 Regression Forest

Regression forest (Breiman, 2001) (RF) is an ensemble of regression decision trees (Breiman, 1984). Recently, the *gradient tree boosting* (Friedman, 2001) has been shown useful in connection with the CMA-ES (Pitra et al., 2018). Therefore, we will focus only on this method.

Let us consider binary regression trees, where each observation \mathbf{x} passes through a series of binary split functions s associated with internal nodes and arrives in the leaf node containing a real-valued constant trained to be the prediction of an associated function value y . Let $\hat{y}_i^{(t)}$ be the prediction of the i -th point of the t -th tree. The t -th tree f_t is obtained in the t -th iteration of the boosting algorithm through optimization of the following function:

$$\mathcal{L}^{(t)} = \sum_{i=1}^N l\left(y_i, \hat{y}_i^{(t-1)} + f_t(\mathbf{x}_i)\right) + \Omega(f_t), \quad \text{where } \Omega(f) = \gamma T_f + \frac{1}{2} \alpha \|w_f\|^2,$$

l is a differentiable convex loss function $l : \mathbb{R}^2 \rightarrow \mathbb{R}$, T_f is the number of leaves in a tree f , w_f are weights of its individual leaves, and $\alpha, \gamma \geq 0$ are penalization constants. The gain can be derived using (9) as follows (see Chen and Guestrin (2016) for details):

$$\mathcal{L}_{\text{split}} = \frac{1}{2} [r(\mathcal{S}_L) + r(\mathcal{S}_R) - r(\mathcal{S}_{L+R})] - \gamma, \quad r(\mathcal{S}) = \frac{\left(\sum_{y \in \mathcal{S}} g(y)\right)^2}{\sum_{y \in \mathcal{S}} h(y) + \alpha}, \quad (9)$$

where set \mathcal{S}_{L+R} is split into \mathcal{S}_L and \mathcal{S}_R , $g(y) = \partial_{\hat{y}^{(t-1)}} l(y, \hat{y}^{(t-1)})$ and $h(y) = \partial_{\hat{y}^{(t-1)}}^2 l(y, \hat{y}^{(t-1)})$ are the first and second order derivatives of the loss function.

The overall boosted forest prediction is obtained through averaging individual tree predictions, where each leaf j in a t -th tree has weight

$$w_j^{(t)} = -\frac{\sum_{y \in \mathcal{S}_j} g(y)}{\sum_{y \in \mathcal{S}_j} h(y) + \alpha}, \quad (10)$$

where \mathcal{S}_j is the set of all training inputs that end in the leaf j . As a prevention of overfitting, the random subsampling of input features or training data can be employed.

2.2 Landscape Features

Let us consider a sample set \mathcal{S} of N pairs of observations in the context of continuous black-box optimization $\mathcal{S} = \{(\mathbf{x}_i, y_i) \in \mathbb{R}^D \times \mathbb{R} \cup \{\circ\} \mid i = 1, \dots, N\}$, where \circ denotes missing y_i value (e. g., \mathbf{x}_i was not evaluated yet). Then the sample set can be utilized to describe landscape properties using a *landscape feature* $\varphi : \bigcup_{N \in \mathbb{N}} \mathbb{R}^{N,D} \times (\mathbb{R} \cup \{\circ\})^{N,1} \mapsto \mathbb{R} \cup \{\pm\infty, \bullet\}$, where \bullet denotes impossibility of feature computation.

A large number of various landscape features have been proposed in recent years in literature. Mersmann et al. (2011) proposed six easy to compute feature sets (each containing a number of individual features for continuous domain) representing different properties: *y-Distribution* set with measures related to the distribution of the objective function values, *Levelset* features capturing the relative position of each value with respect to objective quantiles, *Meta-Model* features extracting the information from linear or quadratic regression models fitted to the sampled data, *Convexity* set describing the level of function landscape convexity, *Curvature* set with gradient and Hessian approximation statistics, and *Local Search* features related to local searches conducted from sampled points. The last three feature sets require additional objective function evaluations.

The *cell-mapping* (CM) approach proposed by Kerschke et al. (2014) discretizes the input space to a user-defined number of blocks (i. e., cells) per dimension. Afterwards, the corresponding features are based on the relations between the cells and points within. Six cell-mapping feature sets were defined: *CM Angle*, *CM Convexity*, *CM Gradient Homogeneity*, *Generalized CM*, *Barrier* and *SOO Trees* by Flamm et al. (2002) and Derbel et al. (2019). It should be noted that CM approach is less useful in higher dimensions where the majority of cells is empty and feature computation can require a lot of time and memory.

Nearest better clustering (NBC) features proposed by Kerschke et al. (2015) are based on the detection of funnel structures. The calculation of such features relies on the comparison of distances from observations to their nearest neighbors and their *nearest better neighbors*, which are the nearest neighbors among the set of all observations with a better objective value. Lunacek and Whitley (2006) proposed the set of *dispersion features* comparing the dispersion among the data points and among subsets of these

points from the sample set. The *information content* features of a continuous landscape by Muñoz et al. (2015a) are derived from methods for calculating the information content of discrete landscapes. In Kerschke (2017), other three feature sets were proposed: *Basic* set with features such as the number of points, search space boundaries or dimension, the proportion of *Principal Components* for a given percentage of variance, coefficients of *Linear Model* fitted in each cell. A comprehensive survey of landscape analysis can be found, e. g., in Muñoz et al. (2015b). A more detailed description of feature sets used in our research can be found in the online available SUPPLEMENTARY MATERIAL¹.

3 Landscape Analysis of Surrogate Models

In recent years, several surrogate-model approaches have been developed to increase the performance of the CMA-ES (cf. the overview in Pitra et al. (2017)). Each such approach has two complementary aspects: the employed regression model and the so called *evolution control* (Jin et al., 2001) managing when to evaluate the model and when the true objective function while replacing the fitness evaluation step on line 4 in Algorithm 1. In Pitra et al. (2021), we have shown a significant influence of the surrogate model on the CMA-ES performance. Thus, we are interested in relationships between the prediction error of surrogate models using various features of the fitness function landscape.

First, we state the problem and research question connected with the relations between surrogate models and landscape features. Then, we present our set of new landscape features based on the CMA-ES state variables. Afterwards, we investigate the properties of landscape features in the context of the training set selection methods and select the most convenient features for further research. Finally, we analyse relationships between the selected features and measured errors of the surrogate models with various settings.

3.1 Problem Statement

The problem can be formalized as follows: In a generation g of a surrogate-assisted version of the CMA-ES, a set of surrogate models \mathcal{M} with hyperparameters θ are trained utilizing particular choices of the training set \mathcal{T} . The training set \mathcal{T} is selected out of an *archive* \mathcal{A} ($\mathcal{T} \subset \mathcal{A}$) containing all points in which the fitness has been evaluated so far, using some TSS method (see Section 2.1.2). Afterwards, \mathcal{M} is tested on the set of points sampled using the CMA-ES distribution $\mathbf{X}_{\text{te}} = \{\mathbf{x}_k | \mathbf{x}_k \sim \mathcal{N}(\mathbf{m}^{(g)}, \sigma^{(g)2} \mathbf{C}^{(g)}), k = 1, \dots, \alpha\}$, where $\alpha \in \mathbb{N}$ depends on the evolution control. The research question connected to this problem is: What relationships between the suitability of different models for predicting the fitness and the considered landscape features do the testing results indicate?

3.2 CMA-ES Landscape Features

To utilize additional information comprised in CMA-ES state variables, we have proposed a set of features based on the CMA-ES (Pitra et al., 2019).

In each CMA-ES generation g during the fitness evaluation step (Step 4), the following additional features φ are obtained for the set of points $\mathbf{X} = \{\mathbf{x}_i\}_{i=1}^N$:

¹https://raw.githubusercontent.com/jdgregorian/surrogate-cmaes-pages/gh-pages/supp/ec2022/supp_mat.pdf

- ◇ **Generation number** $\varphi_{\text{generation}}^{\text{CMA}} = g$ indicates the phase of the optimization process.
- ◇ **Step-size** $\varphi_{\text{step.size}}^{\text{CMA}} = \sigma^{(g)}$ provides an information about the extent of the approximated region.
- ◇ **Number of restarts** $\varphi_{\text{restart}}^{\text{CMA}} = n_r^{(g)}$ performed till generation g may indicate landscape difficulty.
- ◇ **Mahalanobis mean distance** of the CMA-ES mean $\mathbf{m}^{(g)}$ to the sample mean $\mu_{\mathbf{X}}$ of \mathbf{X}

$$\varphi_{\text{mean.dist}}^{\text{CMA}}(\mathbf{X}) = \sqrt{(\mathbf{m}^{(g)} - \mu_{\mathbf{X}})^\top \mathbf{C}_{\mathbf{X}}^{-1} (\mathbf{m}^{(g)} - \mu_{\mathbf{X}})}, \quad (11)$$

where $\mathbf{C}_{\mathbf{X}}$ is the sample covariance of \mathbf{X} . This feature indicates suitability of \mathbf{X} for model training from the point of view of the current state of the CMA-ES algorithm.

- ◇ Square of the \mathbf{p}_c **evolution path length** $\varphi_{\text{evopath.c.norm}}^{\text{CMA}} = \|\mathbf{p}_c^{(g)}\|^2$ is the only possible non-zero eigenvalue of *rank-one update* covariance matrix $\mathbf{p}_c^{(g+1)} \mathbf{p}_c^{(g+1)\top}$ (see Subsection 2.1.1). That feature providing information about the correlations between consecutive CMA-ES steps indicates a similarity of function landscapes among subsequent generations.
- ◇ \mathbf{p}_σ **evolution path ratio**, i. e., the ratio between the evolution path length $\|\mathbf{p}_\sigma^{(g)}\|$ and the expected length of a random evolution path used to update step-size. It provides a useful information about distribution changes:

$$\varphi_{\text{evopath.s.norm}}^{\text{CMA}} = \frac{\|\mathbf{p}_\sigma^{(g)}\|}{\mathbb{E} \|\mathcal{N}(\mathbf{0}, \mathbf{I})\|} = \frac{\|\mathbf{p}_\sigma^{(g)}\| \Gamma(\frac{D}{2})}{\sqrt{2} \Gamma(\frac{D+1}{2})}. \quad (12)$$

- ◇ **CMA similarity likelihood**. The log-likelihood of the set of points \mathbf{X} with respect to the CMA-ES distribution may also serve as a measure of its suitability for training

$$\varphi_{\text{cma.lik}}^{\text{CMA}}(\mathbf{X}) = -\frac{N}{2} \left(D \ln 2\pi\sigma^{(g)^2} + \ln \det \mathbf{C}^{(g)} \right) - \frac{1}{2} \sum_{\mathbf{x} \in \mathbf{X}} \left(\frac{\mathbf{x} - \mathbf{m}^{(g)}}{\sigma^{(g)}} \right)^\top \mathbf{C}^{(g)-1} \left(\frac{\mathbf{x} - \mathbf{m}^{(g)}}{\sigma^{(g)}} \right). \quad (13)$$

3.3 Landscape Features Investigation

Based on the studies in Bajer et al. (2019) and Pitra et al. (2021), we have selected the Doubly trained surrogate CMA-ES (DTS-CMA-ES) (Pitra et al., 2016) as a successful representative of surrogate-assisted CMA-ES algorithms.

During the model training procedure in the DTS-CMA-ES, shown in general in Algorithm 2, a set of training points \mathcal{T} is selected and transformations of \mathbf{X}_{tr} using matrix $\frac{1}{\sigma} \mathbf{C}^{-1/2}$ and \mathbf{y}_{tr} to zero mean and unit variance ($\mathcal{T} = (\mathbf{X}_{\text{tr}}, \mathbf{y}_{\text{tr}})$) are calculated in Steps 2 and 3 before the model hyperparameters θ are fitted. In case of a successful fitting procedure, the resulting model is tested for constancy on an extra generated population due to the CMA-ES restraints against stagnation. Using the same transformation, the points in \mathbf{X}_{te} are transformed before obtaining the model prediction of fitness values $\hat{\mathbf{y}}_{\text{te}}$, which is then inversely transformed to the original output space.

Algorithm 2 Generalized model training in DTS-CMA-ES (Pitra et al., 2016)

Input: \mathcal{A} (archive), TSS (training set selection) method, \mathcal{M} (surrogate model), ψ (model settings), λ (population size), $\mathbf{m}^{(g)}$, $\sigma^{(g)}$, $\mathbf{C}^{(g)}$ (CMA-ES state variables)

- 1: $(\mathbf{X}_{\text{tr}}, \mathbf{y}_{\text{tr}}) \leftarrow$ select points from \mathcal{A} using TSS method
- 2: $\mathbf{X}_{\text{tr}} \leftarrow$ transform \mathbf{X}_{tr} using matrix $\frac{1}{(\sigma^{(g)})^2} \mathbf{C}^{(g)^{-1/2}}$
- 3: $\mathbf{y}_{\text{tr}} \leftarrow$ normalize \mathbf{y}_{tr} to zero mean and unit variance
- 4: $\theta \leftarrow$ fit the hyperparameters of \mathcal{M} using ψ , \mathbf{X}_{tr} , \mathbf{y}_{tr}
- 5: $\mathbf{x}_k^{\text{test}} \leftarrow$ sample $\mathbf{m}^{(g)} + \sigma^{(g)} \mathcal{N}(\mathbf{0}, \mathbf{C}^{(g)})$, $k = 1, \dots, \lambda$ (create testing population)
- 6: $y_k^{\text{test}} \leftarrow \mathcal{M}_\theta(\mathbf{x}_k^{\text{test}})$, $k = 1, \dots, \lambda$ (evaluate testing population using model with hyperparameters θ)
- 7: **if** $\max_k(y_k^{\text{test}}) - \min_k(y_k^{\text{test}}) < \min(10^{-8}, 0.05(\max(\mathbf{y}_{\text{tr}}) - \min(\mathbf{y}_{\text{tr}})))$ **then**
- 8: \mathcal{M}_θ is considered constant $\Rightarrow \mathcal{M}_\theta$ is marked as *not trained*
- 9: **end if**

Output: \mathcal{M}_θ (surrogate model with hyperparameters θ)

3.3.1 Investigation Settings

To investigate landscape features in the context of surrogate-assisted optimization, we have generated² a dataset \mathcal{D} of sample sets using independent runs of the 8 model settings from Pitra et al. (2019) for the DTS-CMA-ES algorithm (Bajer et al., 2019; Pitra et al., 2016) on the 24 noiseless single-objective benchmark functions from the COCO framework (Hansen et al., 2016). All runs were performed in dimensions 2, 3, 5, 10, and 20 on instances 11–15. These instances all stem from the same base problem, and are obtained by translation and/or rotation in the input space and also translation of the objective values. The algorithm runs were terminated if the target fitness value 10^{-8} was reached or the budget of 250 function evaluations per dimension was depleted. Taking into account the double model training in DTS-CMA-ES, we have extracted archives \mathcal{A} and testing sets \mathbf{X}_{te} only from the first model training. The DTS-CMA-ES was employed in the overall best non-adaptive settings from Bajer et al. (2019). To obtain 100 comparable archives and testing sets for landscape features investigation, we have generated a new collection of sample sets \mathcal{D}_{100} , where points for new archives and new populations are created using the weighted sum of original archive distributions from \mathcal{D} . The g -th generated dataset uses the weight vector $\mathbf{w}^{(g)} = \frac{1}{9}(0, \dots, 0, \frac{1}{g-3}, \frac{2}{g-2}, \frac{3}{g-1}, \frac{2}{g}, \frac{1}{g+1}, \frac{0}{g+2}, \frac{0}{g+3}, \dots, 0)^\top$, which provides distribution smoothing across the available generations³. The data from well-known benchmarks were also used by Saini et al. (2019) and Renau et al. (2020).

Because each TSS method in Subsection 2.1.2 results in a different training set \mathcal{T} using identical \mathcal{A} , we have performed all the feature investigations for each TSS method separately. By combining the two *basic sample sets* for feature calculation \mathcal{A} and \mathcal{T} with a population \mathcal{P} consisting of the points without a known value of the original fitness to be evaluated by the surrogate model, we have obtained two new sets $\mathcal{A}_{\mathcal{P}} = \mathcal{A} \cup \mathcal{P}$ and $\mathcal{T}_{\mathcal{P}} = \mathcal{T} \cup \mathcal{P}$. Step 2 of Algorithm 2 performing the transformation of the input could also influence the landscape features. Thus, we have utilized either transformed and

²Source codes covering all mentioned datasets generation and experiments are available on <https://github.com/bajeluk/surrogate-cmaes/tree/meta>.

³The weighted sum of the original archive distributions satisfies $\sum_{n=0}^{g_{\max}} w_n^{(g)} \mathcal{N}(\mathbf{m}^{(n)}, \mathbf{C}^{(n)}) = \mathcal{N}(\sum_{n=0}^{g_{\max}} w_n^{(g)} \mathbf{m}^{(n)}, \sum_{n=0}^{g_{\max}} (w_n^{(g)})^2 \mathbf{C}^{(n)})$, where g_{\max} is the maximal generation reached by the considered original archive and $\mathbf{m}^{(n)}$ and $\mathbf{C}^{(n)}$ are the mean and covariance matrix in CMA-ES generation n .

non-transformed sets for feature calculations, resulting in 8 different sample sets (4 in case of TSS full due to $\mathcal{T} = \mathcal{A}$): $\mathcal{A}, \mathcal{A}^\top, \mathcal{A}_{\mathcal{P}}, \mathcal{A}_{\mathcal{P}}^\top, \mathcal{T}, \mathcal{T}^\top, \mathcal{T}_{\mathcal{P}}, \mathcal{T}_{\mathcal{P}}^\top$, where $^\top$ denotes the transformation.

From each generated run in \mathcal{D}_{100} , we have uniformly selected 100 generations. In each such generations, we have computed all features from the following feature sets for all 3 TSS methods on all sample sets:

<i>Basic</i>	$\Phi_{\text{Basic}},$	<i>Levelset</i>	$\Phi_{\text{Lvl}},$
<i>CMA features</i>	$\Phi_{\text{CMA}},$	<i>Meta-Model</i>	$\Phi_{\text{MM}},$
<i>Dispersion</i>	$\Phi_{\text{Dis}},$	<i>Nearest Better Clustering</i>	$\Phi_{\text{NBC}},$
<i>Information Content</i>	$\Phi_{\text{Inf}},$	<i>y-Distribution</i>	$\Phi_{\text{y-D}}.$

These sets do not require additional evaluations of the objective function and can be computed even in higher dimensions. Some features were not computed due to the following reasons (see Section 2 in SUPPLEMENTARY MATERIAL for feature definitions): From Φ_{Basic} , we have used only φ_{dim} and φ_{obs} because the remaining ones were constant on the whole \mathcal{D}_{100} dataset. φ_{dim} is identical regardless the sample set. φ_{obs} and all features from $\Phi_{\text{y-D}}$ were not computed using the transformation matrix because it does not influence their resulting values. The feature $\varphi_{\text{lin.simple.intercept}}^{\text{MM}} \in \Phi_{\text{MM}}$ was excluded because it is useless if fitness normalization is performed (see Step 3 in Algorithm 2). The remaining features from Φ_{MM} , all the features from Φ_{NBC} , and all three features from $\Phi_{\text{y-D}}$ were not computed on sample sets with \mathcal{P} because it also does not influence their resulting values.

For the rest of the paper, we will consider features which are independent of the sample set (i. e., φ_{dim} and 5 Φ_{CMA} features) as a part of \mathcal{A} -based features only. This results in the total numbers of landscape features equal to 197 for TSS full (all were \mathcal{A} -based) and 388 for TSS nearest and TSS knn (from which 191 features were \mathcal{T} -based).

3.3.2 Feature Analysis Process and Its Results

The results of experiments concerning landscape features are presented in Tables S1–S6 in SUPPLEMENTARY MATERIAL. In the paper, we report only main highlights of the results in Tables 1 and 2.

First, we have investigated the impossibility of feature calculation (i. e., the feature value \bullet) for each feature. Such information can be valuable and we will consider it as a valid output of any feature. On the other hand, large amount of \bullet values on the tested dataset suggests low usability of the respective feature. Therefore, we have excluded features yielding \bullet in more than 25% of all measured values, which were for all TSS methods the feature $\varphi_{\text{eps.s}}^{\text{Inf}}$ on $\mathcal{A}_{\mathcal{P}}, \mathcal{A}_{\mathcal{P}}^\top, \mathcal{T}_{\mathcal{P}},$ and $\mathcal{T}_{\mathcal{P}}^\top$ and for the TSS knn also the features $\varphi_{\text{ratio.mean.02}}^{\text{Dis}}, \varphi_{\text{ratio.median.02}}^{\text{Dis}}, \varphi_{\text{diff.mean.02}}^{\text{Dis}}, \varphi_{\text{diff.median.02}}^{\text{Dis}}$ on $\mathcal{T}, \mathcal{T}^\top, \mathcal{T}_{\mathcal{P}},$ and $\mathcal{T}_{\mathcal{P}}^\top$, as well as $\varphi_{\text{quad.w.interact.adj.r2}}^{\text{MM}}$ on \mathcal{T} and \mathcal{T}^\top . This decreased the numbers of features to 195 for TSS full, 384 for TSS nearest, and 366 for TSS knn. Many features are difficult to calculate using low numbers of points. Therefore, for each feature we have measured the minimal number of points N_\bullet in a particular combination of feature and sample set, for which the calculation resulted in \bullet in at most 1% of cases. All measured values can be found in Tables S1–S6 in SUPPLEMENTARY MATERIAL and values of selected robust features (see below) in Table 2. For the calculation of most of the features, the CMA-ES default population size value in 2D: $N_\bullet = \lambda_{\text{def}} = 4 + \lfloor 3 \ln 2 \rfloor = 6$, or initial point plus doubled default population size in 2D: $N_\bullet = 1 + 2\lambda_{\text{def}} = 13$ was sufficient in all sample sets indexed with \mathcal{P} . Considering sample-set-independent features, no points are needed, because the values concern the CMA-ES iteration or CMA-ES run as

Table 1: Proportion of features for individual TSS with robustness greater or equal to the threshold in the first column. The proportions in brackets represent \mathcal{T} -based features for given TSS (TSS full has only \mathcal{A} -based). The numbers in bold in the grey row are utilized for the following process.

threshold	TSS full	TSS nearest	TSS knn
0.5	125 /195	244 /384 (119/189)	188 /366 (63/171)
0.6	82 /195	158 /384 (76/189)	131 /366 (49/171)
0.7	54 /195	102 /384 (48/189)	93 /366 (39/171)
0.8	43 /195	80 /384 (37/189)	73 /366 (30/171)
0.9	33 /195	60 /384 (27/189)	59 /366 (26/171)
0.99	28 /195	50 /384 (22/189)	30 /366 (2/171)

a whole, not particular points. As can be seen from Tables S1–S6 in SUPPLEMENTARY MATERIAL, the quantile of function values used for splitting the sample set decreases as the dispersion features Φ_{Dis} require more points to be computable ($\varphi \neq \bullet$). For quantile values, see Section 2.3 in SUPPLEMENTARY MATERIAL. Finally, $\varphi_{\text{lin.w.interact.adj.r2}}^{\text{MM}}$ and $\varphi_{\text{quad.w.interact.adj.r2}}^{\text{MM}}$ have also high values of N_{\bullet} , which is plausible taking into account their descriptions (see Section 2.6 in SUPPLEMENTARY MATERIAL).

To increase comparability of investigated features, we normalize all the features to interval $[0, 1]$ using sigmoid function

$$\varphi_{\text{norm}} = \frac{1}{1 + e^{-k(\varphi - \varphi_0)}}, \quad k = \frac{2 \ln 99}{Q_{0.99} - Q_{0.01}}, \quad \varphi_0 = \frac{Q_{0.01} + Q_{0.99}}{2}, \quad (14)$$

where $Q_{0.01}$ and $Q_{0.99}$ are 0.01 and 0.99 quantiles of feature φ on the whole \mathcal{D}_{100} dataset considering values $\varphi \in \mathbb{R} \cup \{\pm\infty\}$. The normalization is derived to map feature quantiles to 0.01 and 0.99, i. e., $\varphi_{\text{norm}}(Q_{0.01}) = 0.01$ and $\varphi_{\text{norm}}(Q_{0.99}) = 0.99$. Such normalization maps infinity values to 0 and 1 and increases comparability of features with large differences in possible values (e. g., $\varphi_{\text{step.size}}^{\text{CMA}} \in [1.5 \cdot 10^{-10}, 1.4 \cdot 10^{15}]$, whereas $\varphi_{\text{nb.cor}}^{\text{NBC}} \in [-1, 1]$).

We have tested the dependency of individual features on the dimension using feature medians from 100 samples for each distribution from \mathcal{D}_{100} . The Friedman’s test rejected the hypothesis that the feature medians are independent of the dimension for all features at the family-wise significance level 0.05 using the Bonferroni-Holm correction. Moreover, for most of the features, the subsequently performed pairwise tests rejected the hypothesis of equality of feature medians for all pairs of dimensions. There were only several features for which the hypothesis was not rejected for some pairs of dimensions (see Tables S1–S6 in SUPPLEMENTARY MATERIAL). Therefore, the influence of the dimension on the vast majority of features is essential.

Our analysis of the influence of multiple landscape features on the predictive error of surrogate models requires high robustness of features against random sampling of points. To have a robust set of k independent features, which return identical values for input in 95% cases, we would like all features to be identical in $100 \sqrt[k]{0.95}\%$ cases. Thus, for our dataset \mathcal{D}_{100} with 100 samples for each distribution even a small k requires all values to be identical, which is almost impossible to achieve for most of the investigated features. Therefore, we define feature *robustness* as a proportion of cases for which the difference between the 1st and 100th percentile calculated after standardization on samples from the same CMA-ES distribution is ≤ 0.05 . Table 1 lists numbers

of features achieving different levels of robustness. We have selected the robustness ≥ 0.9 to be used for subsequent analyses. The robustness calculated for individual features is listed in Tables S1–S6 in SUPPLEMENTARY MATERIAL and its values for features with robustness ≥ 0.9 in Table 2. The chosen level of robustness excluded from further computations all features from Φ_{NBC} and $\Phi_{y\text{-D}}$ for every TSS and all features from Φ_{Inf} for TSS full and TSS nearest. Both Φ_{NBC} and $\Phi_{y\text{-D}}$ are rather sensitive to the input data, where the influence of non-uniform sampling of data is probably not negligible. Features from Φ_{Inf} have very varied robustness. Whereas $\varphi_{\text{eps_max}}^{\text{Inf}}$ provides high robustness around 0.85 on transformed sample sets (up to 0.97 for TSS knn), computations of $\varphi_{m0}^{\text{Inf}}$ and $\varphi_{\text{eps_s}}^{\text{Inf}}$ resulted in the robustness 0.004 and 0.016, respectively, which were the two lowest among all features. The majority of Φ_{CMA} features provided high robustness caused mainly due to the independence of most of the features on the sample set. Features from Φ_{Lvl} based on quadratic discriminant analysis (qda) showed nearly double robustness compared to the rest of Φ_{Lvl} features. The transformation of the input increased robustness of specific types of features from Φ_{Dis} and Φ_{MM} . In particular, it increased the robustness of difference-based features from Φ_{Dis} to more than 0.99 and also of features based on model coefficients from Φ_{MM} . TSS knn is more sample dependent, therefore, the number of points in a sample set can vary. This also decreases the robustness of some ratio-based features. On the other hand, coefficients of simple models from Φ_{MM} show robustness over 0.99 and $\varphi_{\text{cma_mean_dist}}^{\text{CMA}}$ mostly over 0.9. A noticeable dependence of robustness on which of the sets \mathcal{A} , \mathcal{T} , or \mathcal{P} is used was not observed.

The large number of features suggests that for the purpose of investigation of their relationships to surrogate models, they should be clustered into a smaller number of groups of similar features. To this end, we have performed agglomerative hierarchical clustering according to $1 - \sigma_{\text{SW}}(\varphi_i, \varphi_j)$, where σ_{SW} is the *measure* σ by Schweizer and Wolff (1981) and φ_i, φ_j are the vectors of all medians from \mathcal{D}_{100} for the features i and j . To compensate for the ordering-dependency of agglomerative hierarchical clustering, we have performed 5 runs of clustering for each TSS method to find the optimal number of clusters. The number of clusters exceeding a threshold 0.9 for σ_{SW} , averaged over all 15 runs, was 14, that number was subsequently used as the value of k for subsequent k -medoid clustering using again Schweizer-Wolff measure σ as a similarity. The features that are medoids of those 14 clusters are listed in Table 2. Even such a small number of feature representatives can be sufficient for achieving excellent performance in a subsequent investigation (Hoos et al., 2018; Renau et al., 2021). A majority of clusters contain features from the same feature set. Sometimes, the whole cluster is composed of the same features calculated only on different sample sets which suggests that the influence of feature calculation on various sample sets might be negligible in those clusters. On the other hand, feature clusters for TSS knn often all share the base sample set (\mathcal{A} or \mathcal{T}), or the same transformation even if the features are not from the same set of features. Considering the large numbers of available features, it is worth noticing that most of medoids are identical or at least very similar for all TSS methods. TSS full and TSS nearest medoids share identical features, where only 4 (φ_{obs} , $\varphi_{\text{diff_median_02}}^{\text{Dis}}$, $\varphi_{\text{l da_q da_25}}^{\text{Lvl}}$, $\varphi_{\text{quad_simple_cond}}^{\text{MM}}$) differ in the sample set (\mathcal{A} vs. \mathcal{T} , \mathcal{A}^{T} vs. \mathcal{T}^{T} , $\mathcal{A}_{\mathcal{P}}$ vs. $\mathcal{T}_{\mathcal{P}}$, and \mathcal{A}^{T} vs. \mathcal{T}^{T} respectively). Notice that sample sets differ only in using \mathcal{A} or \mathcal{T} . Moreover, 10 out of 14 representatives (φ_{dim} , φ_{obs} , $\varphi_{\text{evopath_s_norm}}^{\text{CMA}}$, $\varphi_{\text{restart}}^{\text{CMA}}$, $\varphi_{\text{cma_lik}}^{\text{CMA}}$, $\varphi_{\text{diff_median_02}}^{\text{Dis}}$, $\varphi_{\text{diff_mean_05}}^{\text{Dis}}$, $\varphi_{\text{l da_q da_10}}^{\text{Lvl}}$, $\varphi_{\text{l da_q da_25}}^{\text{Lvl}}$, $\varphi_{\text{quad_simple_cond}}^{\text{MM}}$) are the same for all considered TSS methods, whereas sample sets utilized for feature calculation sometimes differ. Such similarity can indicate great importance of those features

Table 2: Results of a medoid clustering into 14 clusters of the features for individual TSS methods, according to their Schweizer-Wolf measure σ . The clusters are separated by horizontal lines and their medoid representatives are marked as gray lines. N_{\bullet} denotes the minimal number of points for which the feature calculation resulted in \bullet in at most 1% of cases. The third column shows the robustness — the proportion of measured cases such that the feature values of samples from the same CMA-ES distribution did not differ more than 0.05.

TSS full

	N_{\bullet}	rob.(%)
$\varphi_{\text{obs}}(\mathcal{A})$	1	100.00
$\varphi_{\text{CMA}}^{\text{generation}}$	0	100.00
$\varphi_{\text{obs}}(\mathcal{A}_P)$	13	100.00
$\varphi_{\text{MM}}^{\text{quad.simple.cond}}(\mathcal{A}^T)$	6	95.21
$\varphi_{\text{CMA}}^{\text{cma.lik}}(\mathcal{A})$	1	99.75
$\varphi_{\text{Dis}}^{\text{diff.mean.10}}(\mathcal{A}^T)$	12	99.52
$\varphi_{\text{Dis}}^{\text{diff.mean.25}}(\mathcal{A}^T)$	6	99.55
$\varphi_{\text{CMA}}^{\text{cma.lik}}(\mathcal{A}_P)$	13	99.75
$\varphi_{\text{Dis}}^{\text{diff.mean.10}}(\mathcal{A}_P^T)$	25	99.52
$\varphi_{\text{Dis}}^{\text{diff.mean.25}}(\mathcal{A}_P^T)$	15	99.55
$\varphi_{\text{Dis}}^{\text{diff.mean.05}}(\mathcal{A}^T)$	27	99.49
$\varphi_{\text{Dis}}^{\text{diff.median.05}}(\mathcal{A}^T)$	27	99.46
$\varphi_{\text{Dis}}^{\text{diff.mean.05}}(\mathcal{A}_P^T)$	42	99.49
$\varphi_{\text{Dis}}^{\text{diff.median.05}}(\mathcal{A}_P^T)$	42	99.48
$\varphi_{\text{Dis}}^{\text{diff.median.10}}(\mathcal{A}^T)$	12	99.48
$\varphi_{\text{Dis}}^{\text{diff.median.25}}(\mathcal{A}^T)$	6	99.49
$\varphi_{\text{Dis}}^{\text{diff.median.10}}(\mathcal{A}_P^T)$	25	99.49
$\varphi_{\text{Dis}}^{\text{diff.median.25}}(\mathcal{A}_P^T)$	15	99.50

	N_{\bullet}	rob.(%)
$\varphi_{\text{Dis}}^{\text{diff.mean.02}}(\mathcal{A}^T)$	71	99.52
$\varphi_{\text{Dis}}^{\text{diff.median.02}}(\mathcal{A}^T)$	71	99.44
$\varphi_{\text{Dis}}^{\text{diff.mean.02}}(\mathcal{A}_P^T)$	86	99.52
$\varphi_{\text{Dis}}^{\text{diff.median.02}}(\mathcal{A}_P^T)$	86	99.45
$\varphi_{\text{CMA}}^{\text{restart}}$	0	100.00
$\varphi_{\text{CMA}}^{\text{cma.lik}}(\mathcal{A}^T)$	1	99.96
$\varphi_{\text{CMA}}^{\text{cma.lik}}(\mathcal{A}_P)$	13	99.96
$\varphi_{\text{CMA}}^{\text{evopath.s.norm}}$	0	100.00
$\varphi_{\text{CMA}}^{\text{evopath.c.norm}}$	0	100.00
$\varphi_{\text{Lvl}}^{\text{lda.qda.25}}(\mathcal{A}_P)$	15	94.13
$\varphi_{\text{Lvl}}^{\text{lda.qda.25}}(\mathcal{A}_P^T)$	15	94.12
φ_{dim}	0	100.00
$\varphi_{\text{Lvl}}^{\text{lda.qda.10}}(\mathcal{A}_P)$	18	92.37
$\varphi_{\text{Lvl}}^{\text{lda.qda.10}}(\mathcal{A}_P^T)$	18	92.38
$\varphi_{\text{CMA}}^{\text{step.size}}$	0	100.00

TSS nearest (1/2)

	N_{\bullet}	rob.(%)
$\varphi_{\text{Lvl}}^{\text{lda.qda.10}}(\mathcal{A}_P)$	18	92.37
$\varphi_{\text{Lvl}}^{\text{lda.qda.10}}(\mathcal{A}_P^T)$	18	92.38
$\varphi_{\text{Lvl}}^{\text{lda.qda.10}}(\mathcal{T}_P)$	18	92.37
$\varphi_{\text{Lvl}}^{\text{lda.qda.10}}(\mathcal{T}_P^T)$	18	92.38
$\varphi_{\text{Dis}}^{\text{diff.mean.05}}(\mathcal{A}^T)$	27	99.49
$\varphi_{\text{Dis}}^{\text{diff.median.05}}(\mathcal{A}^T)$	27	99.46
$\varphi_{\text{Dis}}^{\text{diff.mean.05}}(\mathcal{A}_P^T)$	42	99.49
$\varphi_{\text{Dis}}^{\text{diff.median.05}}(\mathcal{A}_P^T)$	42	99.48
$\varphi_{\text{Dis}}^{\text{diff.mean.05}}(\mathcal{T}^T)$	27	99.49
$\varphi_{\text{Dis}}^{\text{diff.median.05}}(\mathcal{T}^T)$	27	99.46
$\varphi_{\text{Dis}}^{\text{diff.mean.05}}(\mathcal{T}_P^T)$	42	99.49
$\varphi_{\text{Dis}}^{\text{diff.median.05}}(\mathcal{T}_P^T)$	42	99.48
$\varphi_{\text{CMA}}^{\text{cma.lik}}(\mathcal{A})$	1	99.75
$\varphi_{\text{Dis}}^{\text{diff.mean.10}}(\mathcal{A}^T)$	12	99.52
$\varphi_{\text{Dis}}^{\text{diff.mean.25}}(\mathcal{A}^T)$	6	99.55
$\varphi_{\text{CMA}}^{\text{cma.lik}}(\mathcal{A}_P)$	13	99.75
$\varphi_{\text{Dis}}^{\text{diff.mean.10}}(\mathcal{A}_P^T)$	25	99.52
$\varphi_{\text{Dis}}^{\text{diff.mean.25}}(\mathcal{A}_P^T)$	15	99.55
$\varphi_{\text{CMA}}^{\text{cma.lik}}(\mathcal{T})$	1	99.75
$\varphi_{\text{Dis}}^{\text{diff.mean.10}}(\mathcal{T}^T)$	12	99.52
$\varphi_{\text{Dis}}^{\text{diff.mean.25}}(\mathcal{T}^T)$	6	99.55
$\varphi_{\text{CMA}}^{\text{cma.lik}}(\mathcal{T}_P)$	13	99.75
$\varphi_{\text{Dis}}^{\text{diff.mean.10}}(\mathcal{T}_P^T)$	25	99.52
$\varphi_{\text{Dis}}^{\text{diff.mean.25}}(\mathcal{T}_P^T)$	15	99.55

	N_{\bullet}	rob.(%)
$\varphi_{\text{Dis}}^{\text{diff.median.10}}(\mathcal{A}^T)$	12	99.48
$\varphi_{\text{Dis}}^{\text{diff.median.25}}(\mathcal{A}^T)$	6	99.49
$\varphi_{\text{Dis}}^{\text{diff.median.10}}(\mathcal{A}_P^T)$	25	99.49
$\varphi_{\text{Dis}}^{\text{diff.median.25}}(\mathcal{A}_P^T)$	15	99.50
$\varphi_{\text{Dis}}^{\text{diff.median.10}}(\mathcal{T}^T)$	12	99.48
$\varphi_{\text{Dis}}^{\text{diff.median.25}}(\mathcal{T}^T)$	6	99.49
$\varphi_{\text{Dis}}^{\text{diff.median.10}}(\mathcal{T}_P^T)$	25	99.49
$\varphi_{\text{Dis}}^{\text{diff.median.25}}(\mathcal{T}_P^T)$	15	99.50
$\varphi_{\text{CMA}}^{\text{evopath.c.norm}}$	0	100.00
$\varphi_{\text{obs}}(\mathcal{A})$	1	100.00
$\varphi_{\text{CMA}}^{\text{generation}}$	0	100.00
$\varphi_{\text{obs}}(\mathcal{A}_P)$	13	100.00
$\varphi_{\text{obs}}(\mathcal{T})$	1	100.00
$\varphi_{\text{obs}}(\mathcal{T}_P)$	13	100.00
$\varphi_{\text{CMA}}^{\text{cma.lik}}(\mathcal{A}^T)$	1	99.96
$\varphi_{\text{CMA}}^{\text{cma.lik}}(\mathcal{A}_P)$	13	99.96
$\varphi_{\text{CMA}}^{\text{cma.lik}}(\mathcal{T}^T)$	1	99.96
$\varphi_{\text{CMA}}^{\text{cma.lik}}(\mathcal{T}_P^T)$	13	99.96
$\varphi_{\text{CMA}}^{\text{evopath.s.norm}}$	0	100.00
φ_{dim}	0	100.00
$\varphi_{\text{CMA}}^{\text{step.size}}$	0	100.00

Table 2: (continued)

TSS nearest (2/2)

	N.	rob.(%)
$\varphi_{\text{MM}}^{\text{quad.simple.cond}}(\mathcal{A}^\top)$	6	95.21
$\varphi_{\text{MM}}^{\text{quad.simple.cond}}(\mathcal{T}^\top)$	6	95.21
$\varphi_{\text{Lvl}}^{\text{lda.qda.25}}(\mathcal{A}_p)$	15	94.13
$\varphi_{\text{Lvl}}^{\text{lda.qda.25}}(\mathcal{A}_p^\top)$	15	94.12
$\varphi_{\text{Lvl}}^{\text{lda.qda.25}}(\mathcal{T}_p)$	15	94.13
$\varphi_{\text{Lvl}}^{\text{lda.qda.25}}(\mathcal{T}_p^\top)$	15	94.12
$\varphi_{\text{restart}}^{\text{CMA}}$	0	100.00

	N.	rob.(%)
$\varphi_{\text{diff.mean.02}}^{\text{Dis}}(\mathcal{A}^\top)$	71	99.52
$\varphi_{\text{diff.median.02}}^{\text{Dis}}(\mathcal{A}^\top)$	71	99.44
$\varphi_{\text{diff.mean.02}}^{\text{Dis}}(\mathcal{A}_p)$	86	99.52
$\varphi_{\text{diff.median.02}}^{\text{Dis}}(\mathcal{A}_p^\top)$	86	99.45
$\varphi_{\text{diff.mean.02}}^{\text{Dis}}(\mathcal{T}^\top)$	71	99.52
$\varphi_{\text{diff.median.02}}^{\text{Dis}}(\mathcal{T}^\top)$	71	99.44
$\varphi_{\text{diff.mean.02}}^{\text{Dis}}(\mathcal{T}_p)$	86	99.52
$\varphi_{\text{diff.median.02}}^{\text{Dis}}(\mathcal{T}_p^\top)$	86	99.45

TSS knn

	N.	rob.(%)
$\varphi_{\text{step.size}}^{\text{CMA}}$	0	100.00
$\varphi_{\text{cma.lik}}^{\text{CMA}}(\mathcal{A})$	1	99.75
$\varphi_{\text{diff.mean.05}}^{\text{Dis}}(\mathcal{A}^\top)$	27	99.49
$\varphi_{\text{diff.median.05}}^{\text{Dis}}(\mathcal{A}^\top)$	27	99.46
$\varphi_{\text{diff.mean.10}}^{\text{Dis}}(\mathcal{A}^\top)$	12	99.52
$\varphi_{\text{diff.median.10}}^{\text{Dis}}(\mathcal{A}^\top)$	12	99.48
$\varphi_{\text{diff.mean.25}}^{\text{Dis}}(\mathcal{A}^\top)$	6	99.55
$\varphi_{\text{diff.median.25}}^{\text{Dis}}(\mathcal{A}^\top)$	6	99.49
$\varphi_{\text{cma.lik}}^{\text{CMA}}(\mathcal{A}_p)$	13	99.75
$\varphi_{\text{diff.mean.05}}^{\text{Dis}}(\mathcal{A}_p^\top)$	42	99.49
$\varphi_{\text{diff.median.05}}^{\text{Dis}}(\mathcal{A}_p^\top)$	42	99.48
$\varphi_{\text{diff.mean.10}}^{\text{Dis}}(\mathcal{A}_p^\top)$	25	99.52
$\varphi_{\text{diff.median.10}}^{\text{Dis}}(\mathcal{A}_p^\top)$	25	99.49
$\varphi_{\text{diff.mean.25}}^{\text{Dis}}(\mathcal{A}_p^\top)$	15	99.55
$\varphi_{\text{diff.median.25}}^{\text{Dis}}(\mathcal{A}_p^\top)$	15	99.50
$\varphi_{\text{lin.simple.coef.max}}^{\text{MM}}(\mathcal{T})$	6	98.12
$\varphi_{\text{cma.mean.dist}}^{\text{CMA}}(\mathcal{T}^\top)$	6	98.40
$\varphi_{\text{cma.mean.dist}}^{\text{CMA}}(\mathcal{T}_p^\top)$	13	98.71
$\varphi_{\text{cma.lik}}^{\text{CMA}}(\mathcal{A}^\top)$	1	99.96
$\varphi_{\text{cma.lik}}^{\text{CMA}}(\mathcal{A}_p^\top)$	13	99.96
$\varphi_{\text{cma.lik}}^{\text{CMA}}(\mathcal{T}^\top)$	1	99.95
$\varphi_{\text{cma.lik}}^{\text{CMA}}(\mathcal{T}_p^\top)$	13	99.96
$\varphi_{\text{cma.lik}}^{\text{CMA}}(\mathcal{T})$	1	98.81
$\varphi_{\text{cma.lik}}^{\text{CMA}}(\mathcal{T}_p)$	13	98.80
φ_{dim}	0	100.00
$\varphi_{\text{evopath.c.norm}}^{\text{CMA}}$	0	100.00
$\varphi_{\text{cma.mean.dist}}^{\text{CMA}}(\mathcal{T}_p)$	13	93.96
$\varphi_{\text{diff.mean.05}}^{\text{Dis}}(\mathcal{T}^\top)$	30	96.80
$\varphi_{\text{diff.median.05}}^{\text{Dis}}(\mathcal{T}^\top)$	30	95.80
$\varphi_{\text{diff.mean.05}}^{\text{Dis}}(\mathcal{T}_p)$	53	96.85
$\varphi_{\text{diff.median.05}}^{\text{Dis}}(\mathcal{T}_p^\top)$	53	95.82

	N.	rob.(%)
$\varphi_{\text{evopath.s.norm}}^{\text{CMA}}$	0	100.00
$\varphi_{\text{lda.qda.25}}^{\text{Lvl}}(\mathcal{A}_p)$	15	94.13
$\varphi_{\text{lda.qda.25}}^{\text{Lvl}}(\mathcal{A}_p^\top)$	15	94.12
$\varphi_{\text{lin.simple.coef.min}}^{\text{MM}}(\mathcal{T})$	6	97.40
$\varphi_{\text{eps.max}}^{\text{Inf}}(\mathcal{T})$	6	97.84
$\varphi_{\text{eps.max}}^{\text{Inf}}(\mathcal{T}_p)$	13	97.70
$\varphi_{\text{quad.simple.cond}}^{\text{MM}}(\mathcal{T})$	6	92.55
$\varphi_{\text{restart}}^{\text{CMA}}$	0	100.00
$\varphi_{\text{diff.mean.10}}^{\text{Dis}}(\mathcal{T}^\top)$	15	96.96
$\varphi_{\text{diff.median.10}}^{\text{Dis}}(\mathcal{T}^\top)$	15	96.09
$\varphi_{\text{diff.mean.25}}^{\text{Dis}}(\mathcal{T}^\top)$	6	97.06
$\varphi_{\text{diff.median.25}}^{\text{Dis}}(\mathcal{T}^\top)$	6	96.27
$\varphi_{\text{diff.mean.10}}^{\text{Dis}}(\mathcal{T}_p^\top)$	28	97.02
$\varphi_{\text{diff.median.10}}^{\text{Dis}}(\mathcal{T}_p^\top)$	28	96.16
$\varphi_{\text{diff.mean.25}}^{\text{Dis}}(\mathcal{T}_p^\top)$	15	97.12
$\varphi_{\text{diff.median.25}}^{\text{Dis}}(\mathcal{T}_p^\top)$	15	96.36
$\varphi_{\text{obs}}(\mathcal{A})$	1	100.00
$\varphi_{\text{generation}}^{\text{CMA}}$	0	100.00
$\varphi_{\text{quad.simple.cond}}^{\text{MM}}(\mathcal{A}^\top)$	6	95.21
$\varphi_{\text{obs}}(\mathcal{A}_p)$	13	100.00
$\varphi_{\text{obs}}(\mathcal{T})$	1	92.16
$\varphi_{\text{obs}}(\mathcal{T}_p)$	13	92.26
$\varphi_{\text{lda.qda.10}}^{\text{Lvl}}(\mathcal{A}_p)$	18	92.37
$\varphi_{\text{lda.qda.10}}^{\text{Lvl}}(\mathcal{A}_p^\top)$	18	92.38
$\varphi_{\text{diff.mean.02}}^{\text{Dis}}(\mathcal{A}^\top)$	71	99.52
$\varphi_{\text{diff.median.02}}^{\text{Dis}}(\mathcal{A}^\top)$	71	99.44
$\varphi_{\text{diff.mean.02}}^{\text{Dis}}(\mathcal{A}_p^\top)$	86	99.52
$\varphi_{\text{diff.median.02}}^{\text{Dis}}(\mathcal{A}_p^\top)$	86	99.45

for characterizing the fitness landscape in the CMA-ES surrogate modeling context.

3.4 Relationships of Landscape Features and Surrogate Models

To investigate the relationships between surrogate model errors and 14 landscape features selected for each TSS in the previous subsection, we have utilized 4 surrogate models: lq, lmm, GPs, and RFs. The latter two models in 8 and 9 different settings respectively. In (Saini et al., 2019), Φ_{MM} features were utilized to investigate connection with several surrogate models in default settings in static scenario only, where the model is selected once for a specific problem regardless the possible following optimization process.

3.4.1 Settings

We have split the dataset \mathcal{D} into validation and testing parts (\mathcal{D}_{val} and \mathcal{D}_{test}) on the covariance function level uniformly at random (considering following levels of \mathcal{D} : dimension, function, instance, covariance function). More specifically, for each dimension, function, and instance in \mathcal{D} , we have uniformly selected runs using 7 covariance functions to \mathcal{D}_{test} and 1 covariance to \mathcal{D}_{val} . In each of those runs, data from 25 uniformly selected generations were used.

The two error measures utilized in our research each follow different aspects of model precision: The *mean-squared error* (MSE) measures how much the model differs directly from the objective function landscape. On the other hand, the *ranking difference error* (RDE) (Bajer et al., 2019) reflects that the CMA-ES state variables are adjusted according to the ordering of μ best points from the current population due to the invariance of the CMA-ES with respect to monotonous transformations. The RDE of $\mathbf{y} \in \mathbb{R}^\lambda$ with respect to $\mathbf{y}' \in \mathbb{R}^\lambda$ considering μ best components is defined:

$$\text{RDE}_\mu(\mathbf{y}, \mathbf{y}') = \frac{\sum_{i, (\rho(\mathbf{y}'))_i \leq \mu} |(\rho(\mathbf{y}'))_i - (\rho(\mathbf{y}))_i|}{\max_\pi \sum_{i=1}^\mu |i - \pi^{-1}(i)|}, \quad (15)$$

where $(\rho(\mathbf{y}))_i$ is the rank of y_i among the components of \mathbf{y} .

The regression model from lmm-CMA was used in its improved version published by Auger et al. (2013). The lmm model operates with the transformation matrix in its own way, thus, the transformation step during training (step 2 in Algorithm 2) is not performed for this model.

The linear-quadratic model was used in the version published by Hansen (2019). The original version utilizes all data without a transformation, therefore, the input data for lq model are not transformed for TSS full.

The GP regression model was employed in the version published by Bajer et al. (2019) using 8 different covariance functions described in Table 3.

The RF model was utilized in 9 different settings described in detail in Table 4.

3.4.2 Results

The results of analysing relationships between landscape features and two error measures for selected surrogate models with the appropriate settings are presented in Figures 1–3, Tables 5 and 6 and Tables S7–S13 in SUPPLEMENTARY MATERIAL.

We have summed up the cases when the model did not provide the prediction, i. e., the error value is not available, in Table 5. Such cases can occur when hyperparameters fitting fails, fitness prediction fails, or the model is considered constant (Steps 4, 6, and 8 in Algorithm 2 respectively). The numbers more or less confirm that more complex methods are more likely to fail. Whereas the lq model, the most simple model among

Table 3: Experimental settings of GP covariances: σ_0^2 – bias constant term, d – metric $d(\mathbf{x}_p, \mathbf{x}_q)$, ℓ – characteristic length-scale, \mathbf{P} – isotropic distance matrix $\mathbf{P} = \ell^{-2}\mathbf{I}$, $\tilde{\mathbf{x}}_p, \tilde{\mathbf{x}}_q$ – inputs augmented by a bias unit, $\ell(\mathbf{x})$ – linear function of \mathbf{x} .

name	covariance function
linear	$\kappa_{\text{LIN}}(\mathbf{x}_p, \mathbf{x}_q) = \sigma_0^2 + \mathbf{x}_p^\top \mathbf{x}_q$
quadratic	$\kappa_{\text{Q}}(\mathbf{x}_p, \mathbf{x}_q) = (\sigma_0^2 + \mathbf{x}_p^\top \mathbf{x}_q)^2$
squared-exponential	$\kappa_{\text{SE}}(d; \sigma_f, \ell) = \sigma_f^2 \exp\left(-\frac{d^2}{2\ell^2}\right)$
Matérn $\frac{5}{2}$	$\kappa_{\text{Mat}}^{\frac{5}{2}}(d; \sigma_f, \ell) = \sigma_f^2 \left(1 + \frac{\sqrt{5}d}{\ell} + \frac{5d^2}{3\ell^2}\right) \exp\left(-\frac{\sqrt{5}d}{\ell}\right)$
rational quadratic	$\kappa_{\text{RQ}}(d; \sigma_f, \ell) = \sigma_f^2 \left(1 + \frac{d^2}{2\ell^2\alpha}\right)^{-\alpha}, \quad \alpha > 0$
neural network	$\kappa_{\text{NN}}(\mathbf{x}_p, \mathbf{x}_q) = \sigma_f^2 \arcsin\left(\frac{2\tilde{\mathbf{x}}_p^\top \mathbf{P} \tilde{\mathbf{x}}_q}{\sqrt{(1+2\tilde{\mathbf{x}}_p^\top \mathbf{P} \tilde{\mathbf{x}}_p)(1+2\tilde{\mathbf{x}}_q^\top \mathbf{P} \tilde{\mathbf{x}}_q)}}\right)$
spatially varying length-scale (Gibbs, 1997)	$\kappa_{\text{Gibbs}}(\mathbf{x}_p, \mathbf{x}_q) = \sigma_f^2 \left(\frac{2\ell(\mathbf{x}_p)\ell(\mathbf{x}_q)}{\ell(\mathbf{x}_p)^2 + \ell(\mathbf{x}_q)^2}\right)^{\frac{D}{2}} \exp\left(-\frac{(\mathbf{x}_p - \mathbf{x}_q)^\top (\mathbf{x}_p - \mathbf{x}_q)}{\ell(\mathbf{x}_p)^2 + \ell(\mathbf{x}_q)^2}\right)$
composite	$\kappa_{\text{SE+Q}} = \kappa_{\text{SE}} + \kappa_{\text{Q}}$

Table 4: Experimental settings of RF for 5 splitting methods found using latin-hypercube design on 100 out of 400 combinations of the number of trees in RF $n_{\text{tree}} \in \{2^6, 2^7, 2^8, 2^9, 2^{10}\}$, the number of points bootstrapped out of N training points $N_t \in \lceil \{1/4, 1/2, 3/4, 1\} \cdot N \rceil$, and the number of randomly subsampled dimensions used for training the individual tree $n_D \in \lceil \{1/4, 1/2, 3/4, 1\} \cdot D \rceil$. The maximum tree depth was set to 8, in accordance with (Chen and Guestrin, 2016). The remaining decision tree parameters have been taken identical to settings from (Pitra et al., 2018). The winning settings on the validation dataset \mathcal{D}_{val} are shown in the format $[n_{\text{tree}}, N_t, n_D]$ (in case of N_t and n_D are shown only the multipliers of N and D respectively). Preliminary testing showed that RFs performance in connection with DTS-CMA-ES is higher when the input data are not transformed to the $\sigma^2\mathbf{C}$ basis. Thus, the transformation step is omitted during model training for both TSS.

TSS	error measure	CART (Breiman, 1984)	SCRT (Dobra and Gehrke, 2002)	OC1 (Murthy et al., 1994)	PAIR (Chaudhuri et al., 1994)	SUPP (Hinton and Revow, 1996)
full	MSE	$[2^{10}, 1, 3/4]$	$[2^8, 1/4, 1/2]$	$[2^7, 1, 1]$	$[2^7, 1, 3/4]$	$[2^7, 1, 1/4]$
	RDE	$[2^6, 3/4, 1]$	$[2^8, 3/4, 1]$	$[2^7, 1, 1]$	$[2^{10}, 3/4, 1]$	$[2^6, 3/4, 1]$
nearest	MSE	$[2^8, 1, 3/4]$	$[2^9, 1/2, 1]$	$[2^7, 1, 1]$	$[2^7, 1, 3/4]$	$[2^{10}, 1/4, 1]$
	RDE	$[2^{10}, 3/4, 1]$	$[2^8, 3/4, 1]$	$[2^7, 1, 1]$	$[2^{10}, 3/4, 1]$	$[2^6, 3/4, 1]$

Table 5: Percentages of cases when the model did not provide usable prediction (model not trained, its prediction failed, or prediction is constant).

TSS	GP								RF								lmm		lq
	Gibbs	LIN	Mat	NN	Q	RQ	SE	SE+Q	CART MSE	CART RDE	SCRT MSE	SCRT RDE	OCI	PAIR MSE	PAIR RDE	SUPP MSE	SUPP RDE		
full	50.3	8.4	26.7	7.6	22.1	5.3	8.5	3.3	5.2	9.6	2.3	20.4	17.9	18.8	2.3	7.0	23.6	8.8	2.5
nearest	40.9	29.5	27.8	24.1	19.8	4.5	7.6	3.1	23.0	22.7	23.4	23.3	23.4	22.9	23.0	23.7	23.1	10.3	2.4
knn	—	—	—	—	—	—	—	—	—	—	—	—	—	—	—	—	—	5.5	—

all tested, provided predictions in almost 98% of all cases, where the missing results can be attributed to constant predictions, the GP model with Gibbs covariance function provided only 55% of the required predictions. Generally, the models were able to provide predictions more often when using TSS full than when using TSS nearest, probably due to the locality of the training set, considering that it is easier to train a constant model on a smaller area, where the differences between objective values are more likely negligible. The TSS knn was the most successful selection method for lmm, probably because it was designed directly for this model. In the following investigation, the cases where the error values were missing for a particular model, were excluded from all comparisons involving that model.

We have tested the statistical significance of the MSE and RDE differences for 19 surrogate model settings using TSS full and TSS nearest methods and also the lmm surrogate model utilizing TSS knn, i. e., 39 different combinations of model settings ψ and TSS methods (ψ , TSS), on all available sample sets using the Friedman test. The resulting p-values of the two Friedman tests, one for each error measure, are below the smallest double precision number. A pairwise comparison of the model settings with respect to MSE and RDE revealed significant differences among the vast majority of pairs of model settings according to the non-parametric two-sided Wilcoxon signed rank test with the Holm correction for the family-wise error. To better illustrate the differences between individual settings, we also count the percentage of cases at which one setting had the error lower than the other. The pairwise score and the statistical significance of the pairwise differences are summarized in Table 6 for RDE and Tables S7 and S8 in SUPPLEMENTARY MATERIAL for both error measures. Results of statistical tests confirmed that the obtained MSE and RDE values are sufficiently diverse for further investigation of model settings suitability. The best overall results were provided by GPs with all covariances except LIN. Especially, GP using SE+Q as a covariance function in TSS nearest significantly outperformed all other (ψ , TSS) combinations. The polynomial models using TSS nearest take the second place in such comparison, being outperformed only by the GP models mentioned above. Generally, models using TSS nearest provided better results than when using TSS full (in case of lmm also better than TSS knn). The percentages of RDE show smaller differences in precision than MSE due to the larger probability of error equality on the limited number of possible RDE values compared to the infinite number of possible MSE values.

To compare the suitability of individual features as descriptors, we separated areas where the surrogate model \mathcal{M} with a particular (ψ , TSS) combination has the best performance. Subsequently, we compared the distributions of each feature value on the whole $\mathcal{D}_{\text{test}}$ with a distribution of each feature value of the selected part using Kolmogorov-Smirnov test (KS test) for MSE and RDE separately. The hypothesis of distribution equality is tested at the family-wise significance level $\alpha = 0.05$ after the

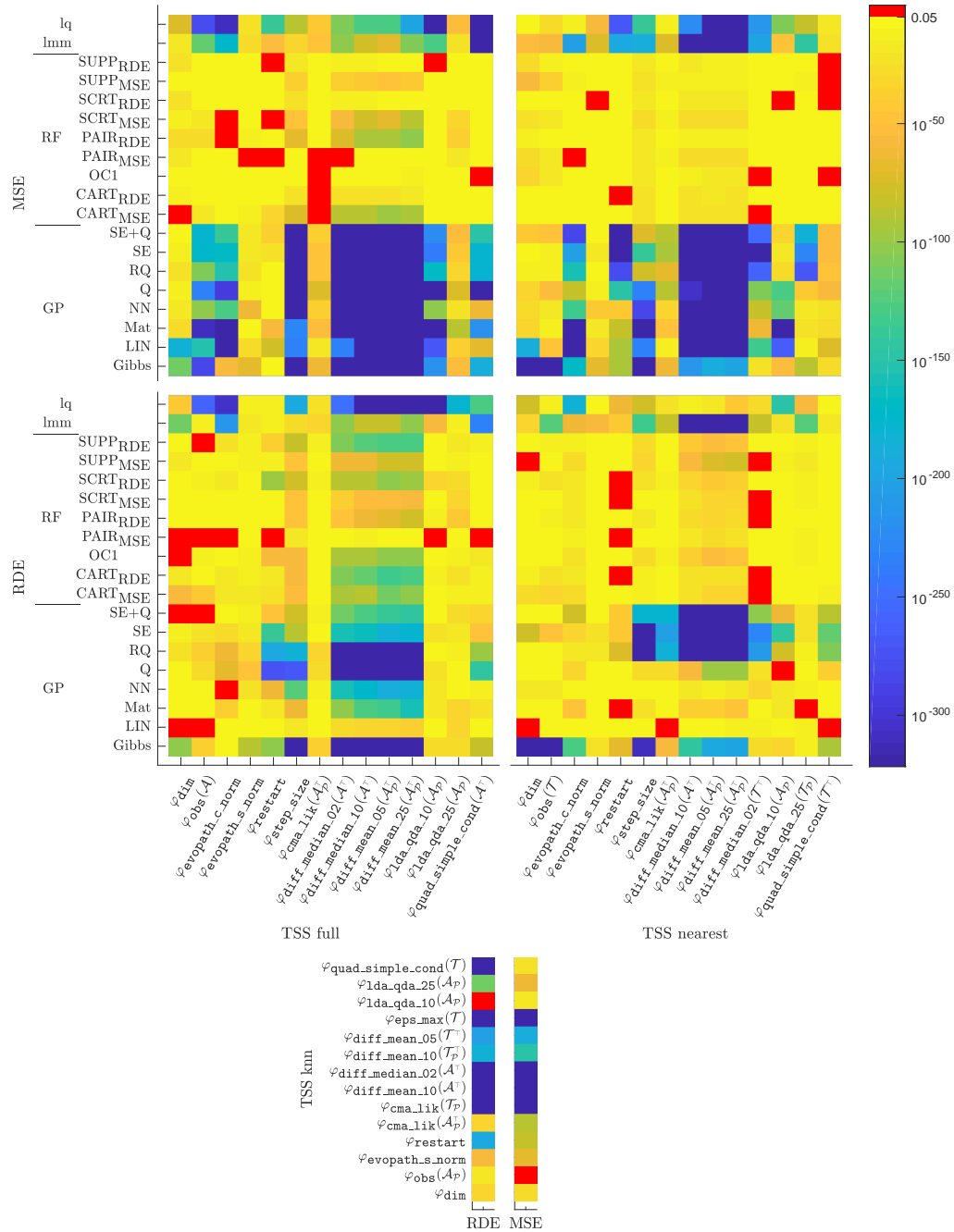


Figure 1: The visualisation of the p-values of the Kolmogorov-Smirnov test comparing the equality of probability distributions of individual features on all data and on those data on which a particular model setting scored best. Non-red colored squares denote KS test results rejecting the equality of distributions with the Holm correction at the family-wise significance level $\alpha = 0.05$, otherwise, p-values are visualised as red squares. TSS knn was employed only in connection with lmm model.

Holm correction. The resulting p-values summarized in Tables S9–S13 in SUPPLEMENTARY MATERIAL and visualised in color in Figure 1 show significant differences in distribution among combinations of model settings and TSS method (ψ , TSS) for the vast majority of considered features. Features from Φ_{Dis} and $\varphi_{\text{step_size}}^{\text{CMA}}$ provided the most significant differences for almost all models. For the GP models and the sample set leading to the lowest MSE, the p-values were often even below the smallest double precision number. These features also provided very low p-values for lmm and lq model. The only exception is $\varphi_{\text{diff_median}_02}^{\text{Dis}}(\mathcal{T}^\top)$ providing notably higher p-values for all model settings. Moreover, features calculated on \mathcal{T} -based sample sets for TSS nearest provided in most cases higher p-values than when calculated on \mathcal{A} -based. From the model point of view, differences of RF model settings are much lower than the rest of settings for all the tested features. This might suggest the lower ability to distinguish between the individual RF settings maybe due to the low performance of these settings on the dataset. The p-values for the MSE and the RDE also differ notably mainly due to the different ranges of values of these two error measures. As its consequence, p-values for MSE more clearly suggest the distinctive power of individual features on model precision, regardless the fact that RDE is more convenient for CMA-ES related problems. Overall, the results of the KS test have shown that there is no tested landscape feature representative for which the selection of the covariance function would be negligible for the vast majority of model settings.

To perform a multivariate statistical analysis we have built two classification trees (CTs): one for TSS full and one for TSS nearest. The data for each TSS method described by 14 features selected in Subsection 3.3 were divided into 19 classes according to which of the 19 considered surrogate model settings achieved the lowest RDE. In case of a tie, the model with the lowest MSE among models with the lowest RDE was the chosen one. The CT trained on those data is the MATLAB implementation of the CART (Breiman, 1984), where the minimal number of cases in leaf was set to 5000, the twoing rule was used as a splitting criterion, φ_{dim} was considered as a discrete variable and the remaining 13 features were considered as continuous. The resulting CTs are depicted in Figures 2 and 3.

The most successful kind of models are GPs, present in most of the leaves proving the leading role shown in pairwise comparisons of model setting errors. Gibbs and $\text{Mat}^{5/2}$ covariances of the GP models constitute the winning GP settings regardless the fact that both provided the lowest numbers of predictions (see Table 5). This is probably caused by the removal of cases where predictions of any model setting were missing. The winning model setting of RF is OC1 method being the most often selected leaf of the CT for TSS full method. The polynomial models are not present in the resulting CT for TSS nearest. The feature $\varphi_{\text{diff_mean}_25}^{\text{Dis}}(\mathcal{A}_p^\top)$ plays possibly the most important role in the CT for TSS full, being in the root node as well as in 4 other nodes, and also very important in the TSS nearest CT, where it is in the root node. This confirms the very strong decisive role of Φ_{Dis} features indicated in the results of KS test. Basic features φ_{dim} and φ_{obs} in few nodes provide the decisions resulting in GP model if both feature values are small and in RF model otherwise. Such dependency coincides with the better ability of RF models to preserve the prediction quality with the growing dimension than the ability of GP models. Features from the Φ_{Lvl} are also very important at least in connection with the TSS nearest. The Φ_{CMA} features are present only in very few nodes. We can observe the connection between the feature $\varphi_{\text{quad_simple_cond}}^{\text{MM}}(\mathcal{A}^\top)$ and the lq model in the CT for TSS full showing the possible ability of Φ_{MM} features to detect convenience of polynomial model usage.

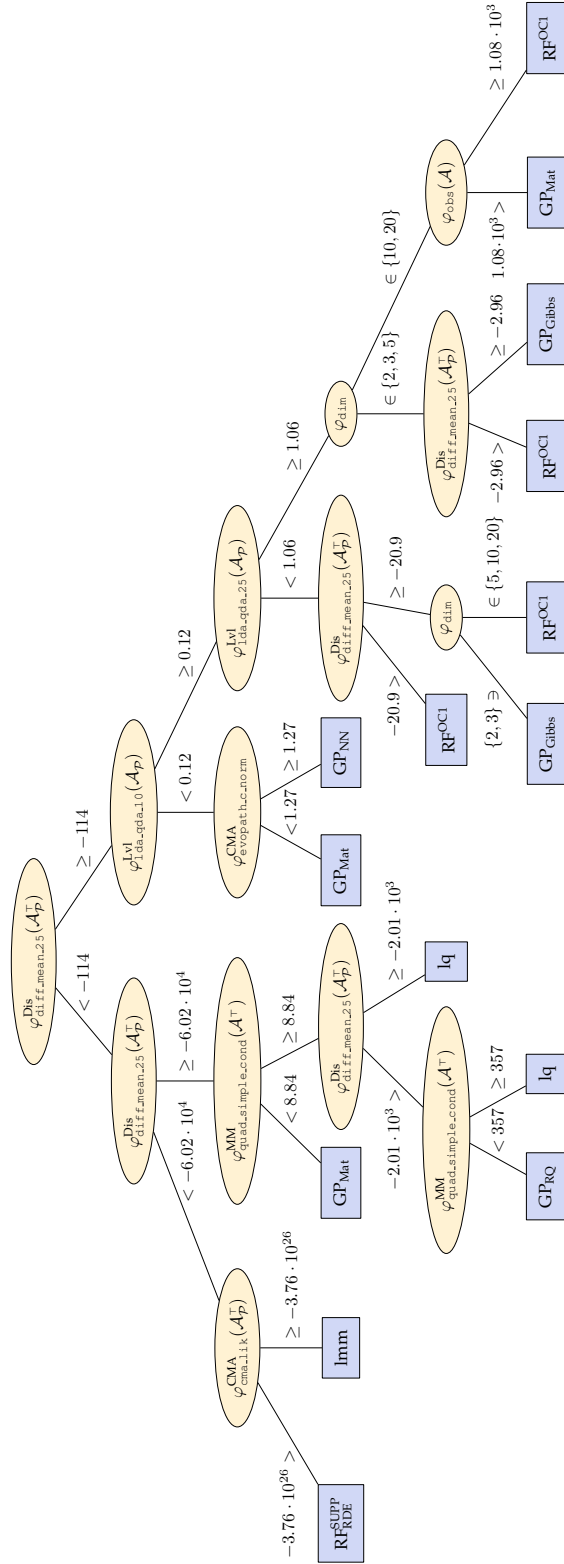


Figure 2: Classification tree analysing the influence of landscape features on the most suitable model and its setting using TSS full.

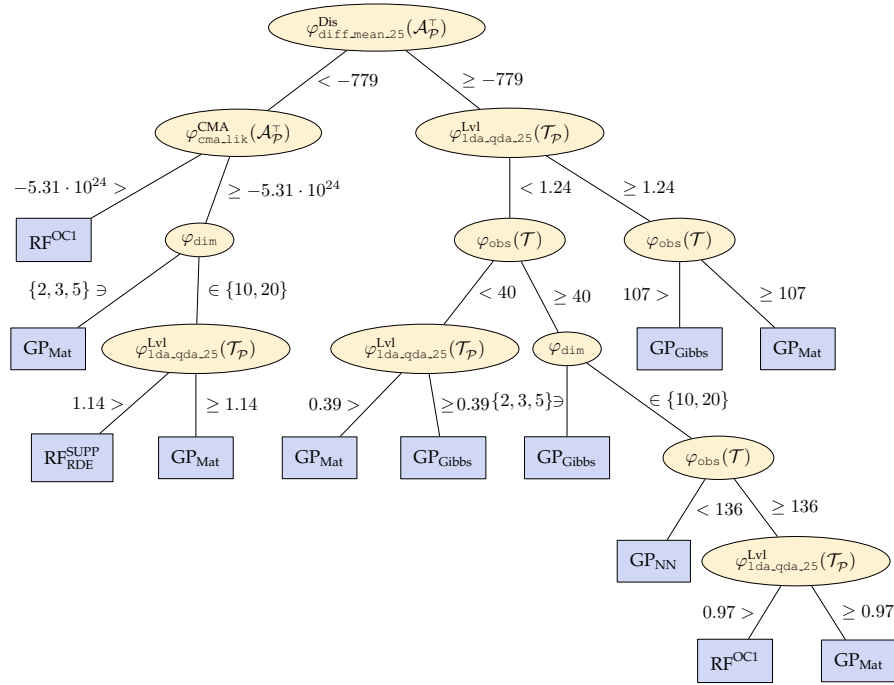


Figure 3: Classification tree analysing the influence of landscape features on the most suitable model and its setting using TSS nearest.

4 Conclusion

This paper has presented a study of relationships between the prediction error of the surrogate models, their settings, and features describing the fitness landscape during evolutionary optimization by the CMA-ES state-of-the-art optimizer for expensive continuous black-box tasks. Four models in 39 different settings for the DTS-CMA-ES, a surrogate-assisted version of the CMA-ES, were compared using three sets of 14 landscape features selected according to their properties, especially according to their robustness and similarity to other features. We analysed MSE and RDE dependence of various models and model settings on the features calculated using three methods selecting sample sets extracted from DTS-CMA-ES runs on noiseless benchmarks from the COCO framework. Up to our knowledge, this analysis of landscape feature properties and their connection to surrogate models in evolutionary optimization is more profound than any other published so far.

Most of the landscape features were designed to be calculated on some initial sample set from the more or less uniform distribution covering the whole search space to easily identify the optimized function and/or the algorithm with the highest performance on such function. In this paper, we operate on a more local level using only data from the actual runs of the optimization algorithm generated in each generation using Gaussian distribution, i. e., data completely different from the original design of those features. Therefore, the low number of robust and mostly similar features confirms the findings of Renau et al. (2020) that the distribution of the initial design has a notable impact on landscape analysis.

The statistical analysis has shown significant differences in the error values among

all 39 model settings using different TSS methods for both MSE and RDE. The GP model settings provided the highest performance followed by polynomial models. Most of the investigated features had distributions on sample sets with particular model settings achieving the lowest error values significantly different from the overall distribution of all data for both error measures and all 3 TSS methods. Finally, the overall results have shown the dispersion features as highly influential on the model settings error values, followed by features based on CMA state variables, features describing the similarity of fitness function to some simple model, features splitting space according to the black-box function values, and simple features such as dimension and number of observations.

The results of this research could be utilized to design a metalearning-based system (Kerschke et al., 2019; Saini et al., 2019) for selection of surrogate models in surrogate-assisted evolutionary optimization algorithms context. The landscape features investigated in this paper are in metalearning known as metafeatures.

References

- Auger, A., Brockhoff, D., and Hansen, N. (2013). Benchmarking the local metamodel CMA-ES on the noiseless BBOB'2013 test bed. *GECCO '13*, pages 1225–1232.
- Auger, A. and Hansen, N. (2005). A restart CMA evolution strategy with increasing population size. volume 2 of *CEC '05*, pages 1769–1776. IEEE.
- Baerns, M. and Holeňa, M. (2009). *Combinatorial Development of Solid Catalytic Materials. Design of High-Throughput Experiments, Data Analysis, Data Mining*. Imperial College Press / World Scientific, London.
- Bajer, L., Pitra, Z., Repický, J., and Holeňa, M. (2019). Gaussian process surrogate models for the CMA Evolution Strategy. *Evolutionary Computation*, 27(4):665–697.
- Breiman, L. (1984). *Classification and regression trees*. Chapman & Hall/CRC.
- Breiman, L. (2001). Random forests. *Machine learning*, 45(1):5–32.
- Büche, D., Schraudolph, N. N., and Koumoutsakos, P. (2005). Accelerating evolutionary algorithms with Gaussian process fitness function models. *IEEE Transactions on Systems, Man, and Cybernetics, Part C*, 35(2):183–194.
- Chaudhuri, P., Huang, M.-C., Loh, W.-Y., and Yao, R. (1994). Piecewise-polynomial regression trees. *Statistica Sinica*, 4(1):143–167.
- Chen, T. and Guestrin, C. (2016). XGBoost: A scalable tree boosting system. *KDD '16*, pages 785–794. ACM.
- Derbel, B., Liefoghe, A., Verel, S., Aguirre, H., and Tanaka, K. (2019). New features for continuous exploratory landscape analysis based on the SOO tree. *FOGA '19*, pages 72–86. ACM.
- Dobra, A. and Gehrke, J. (2002). SECRET: A scalable linear regression tree algorithm. *KDD '02*, pages 481–487. ACM.
- Flamm, C., Hofacker, I. L., Stadler, P. F., and Wolfinger, M. T. (2002). Barrier Trees of Degenerate Landscapes. *Zeitschrift für Physikalische Chemie International Journal of Research in Physical Chemistry and Chemical Physics*, 216(2):155–173.
- Forrester, A. and Keane, A. (2009). Recent advances in surrogate-based optimization. *Progress in Aerospace Sciences*, 45:50–79.
- Friedman, J. H. (2001). Greedy function approximation: A gradient boosting machine. *The Annals of Statistics*, 29(5):1189–1232.

- Gibbs, M. N. (1997). *Bayesian Gaussian Processes for Regression and Classification*. PhD thesis, Department of Physics, University of Cambridge.
- Hansen, N. (2006). The CMA evolution strategy: A comparing review. In *Towards a New Evolutionary Computation*, Studies in Fuzziness and Soft Comp., pages 75–102. Springer.
- Hansen, N. (2019). A global surrogate assisted CMA-ES. GECCO '19, pages 664–672.
- Hansen, N., Auger, A., Mersmann, O., Tusar, T., and Brockhoff, D. (2016). COCO: A platform for comparing continuous optimizers in a black-box setting. arXiv:1603.08785.
- Hansen, N. and Ostermeier, A. (1996). Adapting arbitrary normal mutation distributions in evolution strategies: The covariance matrix adaptation. CEC '96., pages 312–317. IEEE.
- Hinton, G. E. and Revow, M. (1996). Using pairs of data-points to define splits for decision trees. In *Advances in Neural Information Processing Systems*, volume 8, pages 507–513. MIT Press.
- Hoos, H. H., Peitl, T., Slivovsky, F., and Szeider, S. (2018). Portfolio-based algorithm selection for circuit QBFs. CP '18, pages 195–209. Springer.
- Hosder, S., Watson, L., and Grossman, B. (2001). Polynomial response surface approximations for the multidisciplinary design optimization of a high speed civil transport. *Optimization and Engineering*, 2:431–452.
- Jin, Y. (2011). Surrogate-assisted evolutionary computation: Recent advances and future challenges. *Swarm and Evolutionary Computation*, 1:61–70.
- Jin, Y., Olhofer, M., and Sendhoff, B. (2001). Managing approximate models in evolutionary aerodynamic design optimization. CEC '01, pages 592–599. IEEE.
- Kern, S., Hansen, N., and Koumoutsakos, P. (2006). Local Meta-models for Optimization Using Evolution Strategies. PPSN '06, pages 939–948. Springer.
- Kerschke, P. (2017). Comprehensive feature-based landscape analysis of continuous and constrained optimization problems using the R-package flacco. *ArXiv e-prints*.
- Kerschke, P., Hoos, H. H., Neumann, F., and Trautmann, H. (2019). Automated Algorithm Selection: Survey and Perspectives. *Evolutionary Computation*, 27(1):3–45.
- Kerschke, P., Preuss, M., Hernández, C., Schütze, O., Sun, J.-Q., Grimme, C., Rudolph, G., Bischl, B., and Trautmann, H. (2014). Cell mapping techniques for exploratory landscape analysis. EVOLVE V, pages 115–131. Springer.
- Kerschke, P., Preuss, M., Wessing, S., and Trautmann, H. (2015). Detecting funnel structures by means of exploratory landscape analysis. GECCO '15, pages 265–272.
- Kruisselbrink, J., Emmerich, M. T. M., Deutz, A., and Back, T. (2010). A robust optimization approach using Kriging metamodels for robustness approximation in the CMA-ES. CEC '10, pages 1–8. IEEE.
- Lee, H., Jo, Y., Lee, D., and Choi, S. (2016). Surrogate model based design optimization of multiple wing sails considering flow interaction effect. *Ocean Engineering*, 121:422–436.
- Lunacek, M. and Whitley, D. (2006). The dispersion metric and the CMA evolution strategy. GECCO '06, pages 477–484.
- Mersmann, O., Bischl, B., Trautmann, H., Preuss, M., Weihs, C., and Rudolph, G. (2011). Exploratory landscape analysis. GECCO '11, pages 829–836.
- Muñoz, M. A., Kirley, M., and Halgamuge, S. K. (2015a). Exploratory landscape analysis of continuous space optimization problems using information content. *IEEE Transactions on Evolutionary Computation*, 19(1):74–87.

- Muñoz, M. A., Sun, Y., Kirley, M., and Halgamuge, S. K. (2015b). Algorithm selection for black-box continuous optimization problems. *Inf. Sci.*, 317(C):224–245.
- Murthy, S. K., Kasif, S., and Salzberg, S. (1994). A system for induction of oblique decision trees. *J. Artif. Int. Res.*, 2(1):1–32.
- Myers, R., Montgomery, D., and Anderson-Cook, C. (2009). *Response Surface Methodology: Process and Product Optimization Using Designed Experiments*. John Wiley & Sons, Hob.
- Pitra, Z., Bajer, L., and Holeňa, M. (2016). Doubly trained evolution control for the Surrogate CMA-ES. PPSN '16, pages 59–68. Springer.
- Pitra, Z., Bajer, L., Repický, J., and Holeňa, M. (2017). Overview of surrogate-model versions of covariance matrix adaptation evolution strategy. GECCO '17, pages 1622–1629.
- Pitra, Z., Hanuš, M., Koza, J., Tumpach, J., and Holeňa, M. (2021). Interaction between model and its evolution control in surrogate-assisted CMA evolution strategy. GECCO '21, pages 528–536.
- Pitra, Z., Repický, J., and Holeňa, M. (2018). Boosted regression forest for the doubly trained surrogate covariance matrix adaptation evolution strategy. ITAT '18, pages 72–79. CEUR.
- Pitra, Z., Repický, J., and Holeňa, M. (2019). Landscape analysis of Gaussian process surrogates for the covariance matrix adaptation evolution strategy. GECCO '19, pages 691–699.
- Rasheed, K., Ni, X., and Vattam, S. (2005). Methods for using surrogate models to speed up genetic algorithm optimization: Informed operators and genetic engineering. In *Knowledge Incorporation in Evolutionary Computation*, pages 103–123. Springer.
- Rasmussen, C. E. and Williams, C. K. I. (2006). *Gaussian Processes for Machine Learning*. MIT Press.
- Renau, Q., Doerr, C., Dréo, J., and Doerr, B. (2020). Exploratory landscape analysis is strongly sensitive to the sampling strategy. PPSN '20, pages 139–153. Springer.
- Renau, Q., Dréo, J., Doerr, C., and Doerr, B. (2019). Expressiveness and robustness of landscape features. GECCO '19, pages 2048–2051.
- Renau, Q., Dréo, J., Doerr, C., and Doerr, B. (2021). Towards explainable exploratory landscape analysis: Extreme feature selection for classifying BBOB functions. EvoStar '21, pages 17–33.
- Saini, B. S., Lopez-Ibanez, M., and Miettinen, K. (2019). Automatic surrogate modelling technique selection based on features of optimization problems. GECCO '19, pages 1765–1772.
- Schweizer, B. and Wolff, E. F. (1981). On nonparametric measures of dependence for random variables. *Annals of Statistics*, 9(4):879–885.
- Zaefferer, M., Gaida, D., and Bartz-Beielstein, T. (2016). Multi-fidelity modeling and optimization of biogas plants. *Applied Soft Computing*, 48:13–28.

Landscape Analysis for Surrogate Models in the Evolutionary Black-Box Context (Supplementary Material)

Zbyněk Pitra

z.pitra@gmail.com

Faculty of Nuclear Sciences and Physical Engineering, Czech Technical University
Břehová 7, 115 19 Prague, Czech Republic

Jan Koza

koza@cs.cas.cz

Faculty of Information Technology, CTU in Prague,
Thákurova 9, 160 00 Prague 6, Czech Republic

Jiří Tumpach

tumpach@cs.cas.cz

Faculty of Mathematics and Physics, Charles University in Prague,
Malostran. nám. 25, 118 00 Prague, Czech Republic

Martin Holeňa

martin@cs.cas.cz

Institute of Computer Science, Czech Academy of Sciences,
Pod Vodárenskou věží 2, 182 07 Prague, Czech Republic

Abstract

Surrogate modeling has become a valuable technique for black-box optimization tasks with expensive evaluation of the objective function. In this supplementary material for the article *Landscape Analysis for Surrogate Models in the Evolutionary Black-Box Context* (Pitra et al., 2022), we report additional results from the investigation of the relationship between the predictive accuracy of surrogate models and features of the black-box function landscape. We also report additional results from the study of properties of features for landscape analysis in the context of different transformations and ways of selecting the input data.

Keywords

Black-box optimization, Surrogate modeling, Landscape analysis, Metalearning CMA-ES

1 Introduction

In (Pitra et al., 2022) we have presented an investigation of relationships between the prediction error of the surrogate models, their settings, and features describing the fitness landscape during evolutionary optimization by the Covariance Matrix Adaptation Evolution Strategy (CMA-ES) state-of-the-art optimizer for expensive continuous black-box tasks (Hansen and Ostermeier, 1996; Hansen, 2006). Its pseudocode is outlined in Algorithm 1. Four models in 39 different settings for the Doubly Trained Surrogate CMA-ES (DTS-CMA-ES) by Pitra et al. (2016), a surrogate-assisted version of the CMA-ES, were compared using three sets of 14 landscape features selected according to their properties, especially according to their robustness and similarity to other features. We analysed *mean squared error* (MSE) and *ranking difference error* (RDE) (Bajer

Algorithm 1 Pseudocode of the CMA-ES

Input: λ (population-size), \mathbb{b} (fitness function), $(w_i)_{i=1}^\mu$, μ_w (selection and recombination parameters), c_σ , d_σ (step-size control parameters), c_c , c_I , c_μ (covariance matrix adaptation parameters)

- 1: **init** $g = 0$, $\sigma^{(0)} > 0$, $\mathbf{m}^{(0)} \in \mathbb{R}^D$, $\mathbf{C}^{(0)} = \mathbf{I}$, $\mathbf{p}_\sigma^{(0)} = \mathbf{0}$, $\mathbf{p}_c^{(0)} = \mathbf{0}$, $\mu = \lfloor \lambda/2 \rfloor$
 - 2: **repeat**
 - 3: $\mathbf{x}_k \leftarrow \mathbf{m}^{(g)} + \sigma^{(g)} \mathcal{N}(\mathbf{0}, \mathbf{C}^{(g)}) \quad k = 1, \dots, \lambda$
 - 4: $\mathbb{b}_k \leftarrow \mathbb{b}(\mathbf{x}_k) \quad k = 1, \dots, \lambda$
 - 5: $\mathbf{m}^{(g+1)} \leftarrow \sum_{i=1}^\mu w_i \mathbf{x}_{i:\lambda}$, where $\mathbf{x}_{i:\lambda}$ is the i -th best individual out of $\mathbf{x}_1, \dots, \mathbf{x}_\lambda$
 - 6: $\mathbf{p}_\sigma^{(g+1)} \leftarrow (1 - c_\sigma) \mathbf{p}_\sigma^{(g)} + \sqrt{c_\sigma(2 - c_\sigma)\mu_w} \mathbf{C}^{(g)^{-1/2}} \frac{\mathbf{m}^{(g+1)} - \mathbf{m}^{(g)}}{\sigma^{(g)}}$
 - 7: $h_\sigma \leftarrow \mathbb{I} \left(\|\mathbf{p}_\sigma^{(g+1)}\| < \sqrt{1 - (1 - c_\sigma)^{2(g+1)}} \left(1.4 + \frac{2}{D+1} \right) \mathbb{E} \|\mathcal{N}(0, 1)\| \right)$
 - 8: $\mathbf{p}_c^{(g+1)} \leftarrow (1 - c_c) \mathbf{p}_c^{(g)} + h_\sigma \sqrt{c_c(2 - c_c)\mu_w} \frac{\mathbf{m}^{(g+1)} - \mathbf{m}^{(g)}}{\sigma^{(g)}}$
 - 9: $\mathbf{C}_\mu \leftarrow \sum_{i=1}^\mu w_i \sigma^{(g)^{-2}} (\mathbf{x}_{i:\lambda}^{(g+1)} - \mathbf{m}^{(g)}) (\mathbf{x}_{i:\lambda}^{(g+1)} - \mathbf{m}^{(g)})^\top$
 - 10: $\mathbf{C}^{(g+1)} \leftarrow (1 - c_1 - c_\mu) \mathbf{C}^{(g)} + c_1 \mathbf{p}_c^{(g+1)} \mathbf{p}_c^{(g+1)\top} + c_\mu \mathbf{C}_\mu$
 - 11: $\sigma^{(g+1)} \leftarrow \sigma^{(g)} \exp \left(\frac{c_\sigma}{d_\sigma} \left(\frac{\|\mathbf{p}_\sigma^{(g+1)}\|}{\mathbb{E} \|\mathcal{N}(0, \mathbf{I})\|} - 1 \right) \right)$
 - 12: $g \leftarrow g + 1$
 - 13: **until** stopping criterion is met
- Output:** \mathbf{x}_{res} (resulting optimum)

et al., 2019) dependence of various models and model settings on the features calculated using three methods selecting sample sets extracted from DTS-CMA-ES runs on noiseless benchmarks from the Comparing Continuous Optimisers (COCO) testbed (Hansen et al., 2016). Up to our knowledge, this analysis of landscape feature properties and their connection to surrogate models in evolutionary optimization is more profound than any other published so far.

The employed extracted *basic sample sets* were:

- ◊ *archive* \mathcal{A} containing all points evaluated so far by the fitness;
- ◊ *training set* \mathcal{T} selected from \mathcal{A} used for model training.

By combining the two basic sample sets with a population \mathcal{P} consisting of the points without a known value of the fitness to be evaluated by the surrogate model, we have obtained two new sets $\mathcal{A}_\mathcal{P} = \mathcal{A} \cup \mathcal{P}$ and $\mathcal{T}_\mathcal{P} = \mathcal{T} \cup \mathcal{P}$.

The employed training set selection (TSS) methods were:

- ◊ *TSS full*, taking all the already evaluated points, i. e., $\mathcal{T} = \mathcal{A}$,
- ◊ *TSS knn*, selecting the union of the sets of k -nearest neighbors of all points for which the fitness should be predicted, where k is given (e. g., in Kern et al. (2006)),
- ◊ *TSS nearest*, selecting the union of the sets of k -nearest neighbors of all points for which the fitness should be predicted, where k is maximal such that the total number of selected points does not exceed a given maximum number of points N_{\max} and no point is further from current mean $\mathbf{m}^{(g)}$ than a given maximal distance r_{\max} (e. g., in Bajer et al. (2019)).

We have performed all the feature investigations for each TSS method separately.

We have utilized sets either transformed or non-transformed into the $\sigma^2\mathbf{C}$ basis for feature calculations, resulting in 8 different sample sets (4 in case of TSS full due to $\mathcal{T} = \mathcal{A}$): $\mathcal{A}, \mathcal{A}^\top, \mathcal{A}_P, \mathcal{A}_P^\top, \mathcal{T}, \mathcal{T}^\top, \mathcal{T}_P, \mathcal{T}_P^\top$, where $^\top$ denotes the transformation.

The supplementary material is structured as follows. Section 2 describes landscape features utilized in (Pitra et al., 2022) in more detail. Sections 3 and 4 complement the main paper results of testing and analysis, respectively, with more detailed results.

2 Feature Definitions

Let us consider an input set \mathbf{X} of N points in D -dimensional input space

$$\mathbf{X} = \{ \mathbf{x}_i \mid \mathbf{x}_i \in \prod_{j=1}^D [l_j, u_j], l_j, u_j \in \mathbb{R}, l_j < u_j \}_{i=1}^N.$$

Then we can define a *sample set* \mathcal{S} of N pairs of observations

$$\mathcal{S} = \{ (\mathbf{x}_i, y_i) \mid \mathbf{x}_i \in \mathbf{X}, y_i \in \mathbb{R} \cup \{\circ\}, i = 1, \dots, N \},$$

where \circ denotes missing y_i value (e. g., \mathbf{x}_i was not evaluated yet). Then the sample set can be utilized to describe landscape properties using a *landscape feature* φ

$$\varphi : \bigcup_{N \in \mathbb{N}} \mathbb{R}^{N,D} \times (\mathbb{R} \cup \{\circ\})^{N,1} \mapsto \mathbb{R} \cup \{\pm\infty, \bullet\},$$

where \bullet denotes impossibility of feature computation. The y_i values can be gathered to a set $\mathbf{y} = \{y_i\}_{i=1}^N$.

The following features were reimplemented in Matlab according to the R-package `flacco` by Kerschke and Dagefoerde (2017). In the words of Kerschke (2017a), “It is important to notice that, independent of the research domain, most of these features do not provide intuitively understandable numbers. Therefore, we strongly recommend not to interpret them on their own. Moreover, some of them are stochastic and hence should be evaluated multiple times on an instance and afterwards be aggregated in a reasonable manner. Nevertheless, they definitely provide information that can be of great importance to scientific models, such as machine learning algorithms in general or algorithm selectors in particular.” Following the remark about stochasticity, we have fixed random seeds which are not fixed in the original implementation to always return the same values for identical input.

2.1 Basic Features Φ_{Basic}

Kerschke (2017b) summarized the following features providing obvious information about the input space:

- ◇ **Dimension** of the input space $\varphi_{\text{dim}} = D$.
- ◇ **Number of observations** $\varphi_{\text{obs}} = N$.
- ◇ **Minimum and maximum of lower bounds** $\varphi_{\text{lower_min}} = \min_{i \in D} l_i$, $\varphi_{\text{lower_max}} = \max_{i \in D} l_i$.
- ◇ **Minimum and maximum of upper bounds** $\varphi_{\text{upper_min}} = \min_{i \in D} u_i$, $\varphi_{\text{upper_max}} = \max_{i \in D} u_i$.
- ◇ **Minimum and maximum of y values** $\varphi_{\text{objective_min}} = \min_{i \in N} y_i$, $\varphi_{\text{objective_max}} = \max_{i \in N} y_i$.
- ◇ **Minimum and maximum of cell blocks per dimension** $\varphi_{\text{blocks_min}}$, $\varphi_{\text{blocks_max}}$.
- ◇ **Total number of cells** $\varphi_{\text{cells_total}}$.
- ◇ **Number of filled cells** $\varphi_{\text{cells_filled}}$.
- ◇ Binary flag stating whether the **objective function** should be **minimized** $\varphi_{\text{minimize_fun}}$.

In this research, we have used only φ_{dim} and φ_{obs} because the remaining ones were constant on the whole \mathcal{D}_{100} dataset. φ_{dim} is identical regardless the sample set and φ_{obs} was not computed in the $\sigma^2\text{C}$ basis because it does not influence the resulting feature values.

2.2 CMA Features Φ_{CMA}

In each CMA-ES generation g during the fitness evaluation step (Algorithm 1, step 4), we have defined the following features in Pitra et al. (2019) for the set of points \mathbf{X} :

- ◇ **Generation number** $\varphi_{\text{generation}}^{\text{CMA}} = g$ indicates the phase of the optimization process.
- ◇ **Step-size** $\varphi_{\text{step_size}}^{\text{CMA}} = \sigma^{(g)}$ provides an information about the extent of the approximated region.
- ◇ **Number of restarts** $\varphi_{\text{restart}}^{\text{CMA}} = n_r^{(g)}$ performed till generation g may indicate landscape difficulty.
- ◇ **Mahalanobis mean distance** of the CMA-ES mean $\mathbf{m}^{(g)}$ to the sample mean $\mu_{\mathbf{X}}$ of \mathbf{X}

$$\varphi_{\text{mean_dist}}^{\text{CMA}}(\mathbf{X}) = \sqrt{(\mathbf{m}^{(g)} - \mu_{\mathbf{X}})^{\top} \mathbf{C}_{\mathbf{X}}^{-1} (\mathbf{m}^{(g)} - \mu_{\mathbf{X}})}, \quad (1)$$

where $\mathbf{C}_{\mathbf{X}}$ is the sample covariance of \mathbf{X} . This feature indicates suitability of \mathbf{X} for model training from the point of view of the current state of the CMA-ES algorithm.

- ◇ **Square of the \mathbf{p}_c evolution path length** $\varphi_{\text{evopath_c_norm}}^{\text{CMA}} = \|\mathbf{p}_c^{(g)}\|^2$ is the only possible non-zero eigenvalue of *rank-one update* covariance matrix $\mathbf{p}_c^{(g+1)} \mathbf{p}_c^{(g+1)\top}$ (see step 10 in Algorithm 1). That feature providing information about the correlations between consecutive CMA-ES steps indicates a similarity of function landscapes among subsequent generations.
- ◇ **\mathbf{p}_σ evolution path ratio**, i. e., the ratio between the evolution path length $\|\mathbf{p}_\sigma^{(g)}\|$ and the expected length of a random evolution path used to update step-size. It provides a useful information about distribution changes:

$$\varphi_{\text{evopath_s_norm}}^{\text{CMA}} = \frac{\|\mathbf{p}_\sigma^{(g)}\|}{\mathbb{E} \|\mathcal{N}(\mathbf{0}, \mathbf{I})\|} = \frac{\|\mathbf{p}_\sigma^{(g)}\| \Gamma(\frac{D}{2})}{\sqrt{2} \Gamma(\frac{D+1}{2})}. \quad (2)$$

- ◇ **CMA similarity likelihood.** The log-likelihood of the set of points \mathbf{X} with respect to the CMA-ES distribution may also serve as a measure of its suitability for training

$$\begin{aligned} \varphi_{\text{cma_lik}}^{\text{CMA}}(\mathbf{X}) = & -\frac{N}{2} \left(D \ln 2\pi\sigma^{(g)^2} + \ln \det \mathbf{C}^{(g)} \right) \\ & - \frac{1}{2} \sum_{\mathbf{x} \in \mathbf{X}} \left(\frac{\mathbf{x} - \mathbf{m}^{(g)}}{\sigma^{(g)}} \right)^{\top} \mathbf{C}^{(g)-1} \left(\frac{\mathbf{x} - \mathbf{m}^{(g)}}{\sigma^{(g)}} \right). \end{aligned} \quad (3)$$

2.3 Dispersion Features Φ_{Dis}

The dispersion features by Lunacek and Whitley (2006) compare the dispersion among observations from \mathcal{S} and among a subset of these points. The subsets are created based on thresholds using the quantiles 0.02, 0.05, 0.1, and 0.25 of the objective values \mathbf{y} .

The set of all distances within the set \mathcal{S} :

$$D_{\text{all}} = \{\text{dist}(\mathbf{x}_i, \mathbf{x}_j) \mid i, j = 1, \dots, N\}. \quad (4)$$

The quantile subset of all distances:

$$D_{\text{quantile}} = \{\text{dist}(\mathbf{x}_i, \mathbf{x}_j) \mid y_i, y_j \leq Q_{\text{quantile}}(\mathbf{y}), \}. \quad (5)$$

◇ **Ratio of the quantile subset and all points median distances**

$$\varphi_{\text{ratio_median_quantile}}^{\text{Dis}}(\mathcal{S}) = \frac{\text{median } D_{\text{quantile}}}{\text{median } D_{\text{all}}}. \quad (6)$$

◇ **Ratio of the quantile subset and all points mean distances**

$$\varphi_{\text{ratio_mean_quantile}}^{\text{Dis}}(\mathcal{S}) = \frac{\text{mean } D_{\text{quantile}}}{\text{mean } D_{\text{all}}}. \quad (7)$$

◇ **Difference between the quantile subset and all points median distances**

$$\varphi_{\text{diff_median_quantile}}^{\text{Dis}}(\mathcal{S}) = \text{median } D_{\text{quantile}} - \text{median } D_{\text{all}}. \quad (8)$$

◇ **Difference between the quantile subset and all points mean distances**

$$\varphi_{\text{diff_mean_quantile}}^{\text{Dis}}(\mathcal{S}) = \text{mean } D_{\text{quantile}} - \text{mean } D_{\text{all}}. \quad (9)$$

2.4 Information Content Features Φ_{Inf}

The Information Content of Fitness Sequences by Muñoz et al. (2015) approach is based on a symbol sequence $\Psi = \{\psi_1, \dots, \psi_{N-1}\}$, where

$$\psi_i = \begin{cases} \bar{1}, & \text{if } \frac{y_{i+1} - y_i}{\|\mathbf{x}_{i+1} - \mathbf{x}_i\|} < -\varepsilon, \\ 0, & \text{if } \left| \frac{y_{i+1} - y_i}{\|\mathbf{x}_{i+1} - \mathbf{x}_i\|} \right| \leq \varepsilon, \\ 1, & \text{if } \frac{y_{i+1} - y_i}{\|\mathbf{x}_{i+1} - \mathbf{x}_i\|} > \varepsilon. \end{cases} \quad (10)$$

The sequence considers observations from a sample set \mathcal{S} as a random walk across the objective landscape and depends on the information sensitivity parameter $\varepsilon > 0$.

The symbol sequence Ψ is aggregated by the information content $H(\varepsilon) = -\sum_{i \neq j} p_{ij} \log_6 p_{ij}$, where p_{ij} is the probability of having the “block” $\psi_i \psi_j$, where $\psi_i, \psi_j \in \{\bar{1}, 0, 1\}$, within the sequence. Note that the base of the logarithm was set to six as this equals the number of possible blocks $\psi_i \psi_j$ for which $\psi_i \neq \psi_j$, i.e., $\psi_i \psi_j \in \{\bar{1}0, 0\bar{1}, \bar{1}1, 1\bar{1}, 01, 10\}$.

Another aggregation of the information is the so-called partial information content $M(\varepsilon) = |\Psi'|/(N-1)$, where Ψ' is the symbol sequence of alternating $\bar{1}$'s and 1's, which is derived from Ψ by removing all 0 and repeated symbols.

When we do consider \circ as a valid state of y , the sequence Ψ consists of $\psi_i \in \{\bar{1}, 0, 1, \bar{N}\}$, where $\psi_i = \bar{N}$, if $y_{i+1} = \circ$ or $y_i = \circ$. Thus, $H(\varepsilon) = -\sum_{i \neq j} p_{ij} \log_{12} p_{ij}$ due to the increased number of possible $\psi_i \psi_j$ blocks, i.e., $\psi_i \psi_j \in \{\bar{1}0, 0\bar{1}, \bar{1}1, 1\bar{1}, 01, 10, \bar{N}\bar{1}, \bar{1}\bar{N}, \bar{N}0, 0\bar{N}, \bar{N}1, 1\bar{N}\}$. Therefore, features based on Ψ' can be utilized only when \circ state is not present in y .

Based on sequences Ψ and Ψ' the following features can be defined according to Muñoz et al. (2015):

- ◇ **Maximum information content** $\varphi_{h_{\max}}^{\text{Inf}}(\mathcal{S}) = \max_{\varepsilon} H(\varepsilon)$.
- ◇ **Settling sensitivity** $\varphi_{\text{eps}_s}^{\text{Inf}}(\mathcal{S}) = \log_{10} \min(\varepsilon | H(\varepsilon) < s)$, where default $s = 0.05$ (see Muñoz et al. (2015)).
- ◇ **Maximum sensitivity** $\varphi_{\text{eps}_{\max}}^{\text{Inf}}(\mathcal{S}) = \arg \max_{\varepsilon} H(\varepsilon)$.
- ◇ **Initial partial information** $\varphi_{m_0}^{\text{Inf}}(\mathcal{S}) = M(\varepsilon = 0)$.
- ◇ **Ratio of partial information sensitivity** $\varphi_{\text{eps}_{\text{ratio}}}^{\text{Inf}}(\mathcal{S}) = \log_{10} \max(\varepsilon | M(\varepsilon) > r \varphi_{m_0}^{\text{Inf}}(\mathcal{S}))$, where default $r = 0.5$ (see also Muñoz et al. (2015)).

2.5 Levelset Features Φ_{Lvl}

In Levelset features by Mersmann et al. (2011), the sample set \mathcal{S} is split into two classes by a specific threshold calculated using the quantiles 0.1, 0.25, and 0.5. Linear, quadratic, and mixture discriminant analysis (`lda`, `qda`, and `mda`) are used to predict whether the objective values y fall below or exceed the calculated threshold. The extracted features are based on the distribution of the resulting cross-validated mean misclassification errors of each classifier.

- ◇ **Mean misclassification error** of an appropriate discriminant analysis `method` using defined quantile $\varphi_{\text{mmce-}[method]-[quantile]}^{Lvl}(\mathcal{S})$.
- ◇ **Ratio between mean misclassification errors** of two discriminant analysis methods using a given quantile $\varphi_{\text{[method1]-[method2]-[quantile]}^{Lvl}(\mathcal{S})$.

2.6 Metamodel Features Φ_{MM}

To calculate metamodel features by Mersmann et al. (2011), linear and quadratic regression models (`lin` and `quad`) with or without interactions are fitted to a sample set \mathcal{S} . The adjusted coefficient of determination R^2 and features reflecting the size relations of the model coefficients are extracted:

- ◇ **Adjusted R^2 of a simple model** $\varphi_{[\text{model}].\text{simple_adj_r2}}^{MM}(\mathcal{S})$.
- ◇ **Adjusted R^2 of a model with interactions** $\varphi_{[\text{model}].\text{w_interact_adj_r2}}^{MM}(\mathcal{S})$.
- ◇ **Intercept of a simple linear model** $\varphi_{\text{lin.simple.intercept}}^{MM}(\mathcal{S})$.
- ◇ **Minimal absolute value of linear model coefficients** $\varphi_{\text{lin.simple.coef.min}}^{MM}(\mathcal{S})$.
- ◇ **Maximal absolute value of linear model coefficients** $\varphi_{\text{lin.simple.coef.max}}^{MM}(\mathcal{S})$.
- ◇ **Ratio of maximal and minimal abs. value of linear model coefficients** $\varphi_{\text{lin.simple.coef.max.by.min}}^{MM}(\mathcal{S})$.
- ◇ **Ratio of maximal and minimal abs. value of quadratic model coefficients** $\varphi_{\text{quad.simple.cond}}^{MM}(\mathcal{S})$.

The feature $\varphi_{\text{lin.simple.intercept}}^{MM}$ was excluded because it is useless if fitness normalization is performed. The remaining features were not computed on sample sets with \mathcal{P} because it does not influence the resulting feature values.

2.7 Nearest Better Clustering Features Φ_{NBC}

Nearest better clustering features by Kerschke et al. (2015) extract information based on the comparison of the sets of distances from all observations towards their nearest neighbors (D_{nn}) and their nearest better neighbors (D_{nb}).

The distance to the nearest neighbor of a search point \mathbf{x}_i , $i = 1, \dots, N$ from a set of points \mathbf{X} :

$$d_{\text{nn}}(\mathbf{x}_i, \mathbf{X}) = \min(\text{dist}(\mathbf{x}_i, \mathbf{x}_j) | \mathbf{x}_j \in \mathbf{X}, i \neq j). \quad (11)$$

The distance to the nearest better neighbor:

$$d_{\text{nb}}(\mathbf{x}_i, \mathbf{X}) = \min(\text{dist}(\mathbf{x}_i, \mathbf{x}_j) | y_j < y_i, \mathbf{x}_j \in \mathbf{X}). \quad (12)$$

The set of all nearest neighbor distances within the set \mathbf{X} :

$$D_{\text{nn}} = \{d_{\text{nn}}(\mathbf{x}_i, \mathbf{X}) | i = 1, \dots, N\}. \quad (13)$$

The set of all nearest better distances:

$$D_{\text{nb}} = \{d_{\text{nb}}(\mathbf{x}_i, \mathbf{X}) | i = 1, \dots, N\}. \quad (14)$$

The features are defined as follows:

- ◇ **Ratio of the standard deviations** between the D_{nn} and D_{nb} $\varphi_{\text{nb_std_ratio}}^{\text{NBC}}(\mathcal{S}) = \frac{\text{std } D_{\text{nn}}}{\text{std } D_{\text{nb}}}$.
- ◇ **Ratio of the means** between the D_{nn} and D_{nb} $\varphi_{\text{nb_mean_ratio}}^{\text{NBC}}(\mathcal{S}) = \frac{\text{mean } D_{\text{nn}}}{\text{mean } D_{\text{nb}}}$.
- ◇ **Correlation between the distances** of the nearest neighbors and nearest better neighbors $\varphi_{\text{nb_cor}}^{\text{NBC}}(\mathcal{S}) = \text{corr}(D_{\text{nn}}, D_{\text{nb}})$.
- ◇ **Coefficient of variation of the distance ratios** $\varphi_{\text{dist_ratio}}^{\text{NBC}}(\mathcal{S}) = \frac{\text{std } \mathcal{W}}{\text{mean } \mathcal{W}}$, where $\mathcal{W} = \left\{ \frac{d_{\text{nn}}(\mathbf{x}, \mathbf{X})}{d_{\text{nb}}(\mathbf{x}, \mathbf{X})} \mid \mathbf{x} \in \mathbf{X} \right\}$.
- ◇ **Correlation between the fitness value, and the count of observations** to whom the current observation is the nearest better neighbor $\varphi_{\text{nb_fitness_cor}}^{\text{NBC}}(\mathcal{S}) = -\text{corr}(\{\text{deg}^-(\mathbf{x}_i), y_i | i = 1, \dots, N\})$, where $\text{deg}^-(\mathbf{x}_i)$ is the indegree of \mathbf{x}_i in the nearest better graph (the number of points for which a certain point is the nearest better point).

The features from Φ_{NBC} were not computed on sample sets with \mathcal{P} because it does not influence the resulting feature values.

2.8 \mathbf{y} -Distribution Features $\Phi_{\mathbf{y-D}}$

The \mathbf{y} -distribution features from Mersmann et al. (2011) compute the basic statistics of the fitness values \mathbf{y} .

- ◇ **Skewness and kurtosis** of \mathbf{y} values $\varphi_{\text{skewness}}^{\mathbf{y-D}}(\mathbf{y})$ and $\varphi_{\text{kurtosis}}^{\mathbf{y-D}}(\mathbf{y})$.
- ◇ **Number of peaks** of the kernel-based estimation of the density of \mathbf{y} -distribution $\varphi_{\text{number_of_peaks}}^{\mathbf{y-D}}(\mathbf{y})$, where the peak is defined according to Kerschke and Dageforde (2017).

All three features were computed only on \mathcal{A} and \mathcal{T} because neither \mathcal{P} nor the $\sigma^2\mathbf{C}$ basis influence the resulting feature values.

3 Landscape Feature Investigation Results

First, we have investigated the impossibility of feature calculation (i. e., the feature value \bullet) for each feature. Considering that large amount of \bullet values on the tested dataset suggests low usability of the respective feature, we have excluded features yielding \bullet in more than 25% of all measured values. Many features are difficult to calculate using low numbers of points. Therefore, for each feature we have measured the minimal number of points N_{\bullet} in a particular combination of feature and sample set, for which the calculation resulted in \bullet in at most 1% of cases. All measured values can be found in Tables S1–S6.

We have tested the dependency of individual features on the dimension using feature medians from 100 samples for each distribution from the dataset. The Friedman’s test rejected the hypothesis that the feature medians are independent of the dimension for all features at the family-wise significance level 0.05 using the Bonferroni-Holm correction. Moreover, for most of the features, the subsequently performed pairwise tests rejected the hypothesis of equality of feature medians for all pairs of dimensions. There were only several features for which the hypothesis was not rejected for some pairs of dimensions (see Tables S1–S6).

Any analysis of the influence of multiple landscape features on the predictive error of surrogate models requires high robustness of features against random sampling of points. Therefore, we define feature *robustness* as a proportion of cases for which the difference between the 1st and 100th percentile calculated after standardization on samples from the same CMA-ES distribution is ≤ 0.05 . The robustness calculated for individual features is listed in Tables S1–S6.

Table S1: TSS full features ($\mathcal{A} = \mathcal{T}$ for TSS full) from feature sets Φ_{Basic} , Φ_{CMA} , Φ_{Dis} , and $\Phi_{\text{y-D}}$. Features are grouped according to their feature sets (separated by horizontal lines). Features with less than 25% of values equal to \bullet and robustness greater than 0.9, are in gray. N_{\bullet} denotes the lowest measured number of points from which at most 1% of feature calculations resulted in \bullet ($N_{\bullet} = 0$ for sample set independent φ). The (D_i, D_j) column shows the pairs of feature dimensions for which the two-sided Wilcoxon signed rank test with the Bonferroni-Holm correction does not reject the hypothesis of equality of median feature values, at the family-wise level 0.05 for each individual feature.

	\mathcal{A}			\mathcal{A}^{\top}			$\mathcal{A}_{\mathcal{P}}$			$\mathcal{A}_{\overline{\mathcal{P}}}$		
	N_{\bullet}	rob.(%)	(D_i, D_j)	N_{\bullet}	rob.(%)	(D_i, D_j)	N_{\bullet}	rob.(%)	(D_i, D_j)	N_{\bullet}	rob.(%)	(D_i, D_j)
φ_{dim}	0	100.00		0	100.00		0	100.00		0	100.00	
φ_{obs}	1	100.00		1	100.00		13	100.00		13	100.00	
$\varphi_{\text{CMA}}^{\text{generation}}$	0	100.00		0	100.00		0	100.00		0	100.00	
$\varphi_{\text{CMA}}^{\text{step.size}}$	0	100.00		0	100.00		0	100.00		0	100.00	
$\varphi_{\text{CMA}}^{\text{restart}}$	0	100.00		0	100.00		0	100.00		0	100.00	
$\varphi_{\text{CMA}}^{\text{mean.dist}}$	6	70.11		6	56.83		13	63.61		13	54.12	
$\varphi_{\text{CMA}}^{\text{evopath.c.norm}}$	0	100.00		0	100.00		0	100.00		0	100.00	
$\varphi_{\text{CMA}}^{\text{evopath.s.norm}}$	0	100.00		0	100.00		0	100.00		0	100.00	
$\varphi_{\text{CMA}}^{\text{lik}}$	1	99.75		1	99.96		13	99.75		13	99.96	
$\varphi_{\text{Dis}}^{\text{ratio.mean.02}}$	71	57.69	(2, 5), (3, 10), (3, 20)	71	62.33	(2, 5), (5, 20)	86	57.36	(2, 5), (3, 20)	86	62.16	
$\varphi_{\text{Dis}}^{\text{ratio.median.02}}$	71	65.95	(3, 5)	71	69.28		86	65.41		86	69.60	
$\varphi_{\text{Dis}}^{\text{diff.mean.02}}$	71	47.75		71	99.52		86	48.77		86	99.52	
$\varphi_{\text{Dis}}^{\text{diff.median.02}}$	71	50.21		71	99.44		86	51.44		86	99.45	
$\varphi_{\text{Dis}}^{\text{ratio.mean.05}}$	27	55.22	(5, 20)	27	60.59		42	54.76	(5, 20)	42	60.32	
$\varphi_{\text{Dis}}^{\text{ratio.median.05}}$	27	59.80		27	64.43		42	59.66	(5, 20)	42	64.57	
$\varphi_{\text{Dis}}^{\text{diff.mean.05}}$	27	47.99		27	99.49		42	49.16		42	99.49	
$\varphi_{\text{Dis}}^{\text{diff.median.05}}$	27	51.16		27	99.46		42	52.88		42	99.48	
$\varphi_{\text{Dis}}^{\text{ratio.mean.10}}$	12	54.63	(5, 20)	12	59.33		25	54.06	(5, 20)	25	58.71	
$\varphi_{\text{Dis}}^{\text{ratio.median.10}}$	12	58.29		12	62.38	(2, 3)	25	57.80		25	61.82	
$\varphi_{\text{Dis}}^{\text{diff.mean.10}}$	12	49.70		12	99.52		25	50.88		25	99.52	
$\varphi_{\text{Dis}}^{\text{diff.median.10}}$	12	53.51		12	99.48		25	55.53		25	99.49	
$\varphi_{\text{Dis}}^{\text{ratio.mean.25}}$	6	54.80		6	58.86		15	53.87		15	58.06	
$\varphi_{\text{Dis}}^{\text{ratio.median.25}}$	6	56.21		6	59.74		15	54.91		15	58.26	
$\varphi_{\text{Dis}}^{\text{diff.mean.25}}$	6	53.78		6	99.55		15	55.29		15	99.55	
$\varphi_{\text{Dis}}^{\text{diff.median.25}}$	6	57.40		6	99.49		15	60.24		15	99.50	
$\varphi_{\text{y-D}}^{\text{skewness}}$	6	36.71		–	–	–	–	–	–	–	–	–
$\varphi_{\text{y-D}}^{\text{kurtosis}}$	6	63.06		–	–	–	–	–	–	–	–	–
$\varphi_{\text{y-D}}^{\text{number.of.peaks}}$	6	32.34		–	–	–	–	–	–	–	–	–

Table S2: TSS full features ($\mathcal{A} = \mathcal{T}$ for TSS full) from feature sets Φ_{Lvl} , Φ_{MM} , Φ_{Inf} , and Φ_{NBC} . Features are grouped according to their feature sets (separated by horizontal lines). Features with less than 25% of values equal to \bullet and robustness greater than 0.9, are in gray. N_{\bullet} denotes the lowest measured number of points from which at most 1% of feature calculations resulted in \bullet ($N_{\bullet} = 0$ for sample set independent φ). The (D_i, D_j) column shows the pairs of feature dimensions for which the two-sided Wilcoxon signed rank test with the Bonferroni-Holm correction does not reject the hypothesis of equality of median feature values, at the family-wise level 0.05 for each individual feature.

	\mathcal{A}			\mathcal{A}^{\top}			$\mathcal{A}_{\mathcal{P}}$			$\mathcal{A}_{\mathcal{P}}^{\top}$		
	N_{\bullet}	rob.(%)	(D_i, D_j)	N_{\bullet}	rob.(%)	(D_i, D_j)	N_{\bullet}	rob.(%)	(D_i, D_j)	N_{\bullet}	rob.(%)	(D_i, D_j)
$\varphi_{mmce.lda.10}$	6	39.47		6	39.47		13	53.01		13	53.01	
$\varphi_{mmce.qda.10}$	6	69.30		6	69.88		13	65.30		13	65.91	
$\varphi_{mmce.mda.10}$	6	28.07		6	28.14		13	27.38		13	27.64	
$\varphi_{lda.qda.10}$	6	80.09		6	80.12		18	92.37		18	92.38	
$\varphi_{lda.mda.10}$	6	44.32		6	42.71		13	46.42		13	48.00	
$\varphi_{qda.mda.10}$	6	81.14		6	80.51		13	78.27		13	77.33	
$\varphi_{mmce.lda.25}$	6	32.64		6	32.64		13	54.19		13	54.19	
$\varphi_{mmce.qda.25}$	6	62.01		6	62.41		13	56.49		13	56.69	
$\varphi_{mmce.mda.25}$	6	22.86		6	22.63		13	27.03		13	26.99	
$\varphi_{lda.qda.25}$	6	76.25		6	76.29	(3, 5)	15	94.13		15	94.12	
$\varphi_{lda.mda.25}$	6	32.07	(3, 20)	6	27.68	(3, 10), (10, 20)	13	22.86		13	20.39	
$\varphi_{qda.mda.25}$	6	77.24		6	77.68		13	63.08		13	63.11	
$\varphi_{mmce.lda.50}$	6	22.40		6	22.39		13	18.46		13	18.46	
$\varphi_{mmce.qda.50}$	6	48.24		6	49.46		13	32.88		13	33.15	
$\varphi_{mmce.mda.50}$	6	20.13		6	19.60		13	38.52		13	37.58	
$\varphi_{lda.qda.50}$	6	69.22	(10, 20)	6	69.24	(10, 20)	15	84.45		15	84.41	
$\varphi_{lda.mda.50}$	6	36.05		6	30.90		13	6.80	(5, 20)	13	4.51	
$\varphi_{qda.mda.50}$	6	42.65	(3, 20)	6	40.68		13	21.96	(5, 20)	13	22.47	(3, 5), (5, 20)
$\varphi_{lin.simple.adj.r2}$	6	19.64		6	19.62		—	—	—	—	—	—
$\varphi_{lin.simple.coef.min}$	6	51.95		6	85.41		—	—	—	—	—	—
$\varphi_{lin.simple.coef.max}$	6	29.73		6	77.68		—	—	—	—	—	—
$\varphi_{lin.simple.coef.max.by.min}$	6	27.78		6	69.78		—	—	—	—	—	—
$\varphi_{lin.w.interact.adj.r2}$	100	44.77		100	43.89		—	—	—	—	—	—
$\varphi_{quad.simple.adj.r2}$	6	50.23		6	52.16		—	—	—	—	—	—
$\varphi_{quad.simple.cond}$	6	46.45		6	95.21		—	—	—	—	—	—
$\varphi_{quad.w.interact.adj.r2}$	629	82.50		531	77.81		—	—	—	—	—	—
$\varphi_{h.max}$	6	14.46	(3, 5)	6	33.83		13	35.74		13	35.42	
φ_{inf}	6	6.59		6	34.65		3056	26.05		3196	54.56	
$\varphi_{eps.s}$	6	64.93		6	84.99		13	65.17		13	84.18	
$\varphi_{eps.max}$	6	1.30		6	3.88		—	—	—	—	—	—
φ_{inf}	6	27.67		6	44.91		—	—	—	—	—	—
$\varphi_{eps.ratio}$	6	31.11		6	18.27		—	—	—	—	—	—
φ_{NBC}	6	38.98		6	32.96		—	—	—	—	—	—
φ_{NBC}	6	45.94		6	32.39		—	—	—	—	—	—
φ_{NBC}	6	55.23		6	50.78		—	—	—	—	—	—
φ_{NBC}	6	77.17		6	77.13		—	—	—	—	—	—

Table S3: TSS nearest features from feature sets Φ_{Basic} , Φ_{CMA} , Φ_{Dis} , and $\Phi_{y\text{-D}}$ (only \mathcal{T} -based and sample set indepent, \mathcal{A} -based are identical to TSS full in Table S1). Features are grouped according to their feature sets (separated by horizontal lines). Features with less than 25% of values equal to \bullet and robustness greater than 0.9, are in gray. N_{\bullet} denotes the lowest measured number of points from which at most 1% of feature calculations resulted in \bullet ($N_{\bullet} = 0$ for sample set independent φ). The (D_i, D_j) column shows the pairs of feature dimensions for which the two-sided Wilcoxon signed rank test with the Bonferroni-Holm correction does not reject the hypothesis of equality of median feature values, at the family-wise level 0.05 for each individual feature.

	\mathcal{T}			\mathcal{T}^{\top}			$\mathcal{T}_{\mathcal{P}}$			$\mathcal{T}_{\mathcal{P}}^{\top}$		
	N_{\bullet}	rob.(%)	(D_i, D_j)	N_{\bullet}	rob.(%)	(D_i, D_j)	N_{\bullet}	rob.(%)	(D_i, D_j)	N_{\bullet}	rob.(%)	(D_i, D_j)
φ_{dim}	0	100.00		0	100.00		0	100.00		0	100.00	
φ_{obs}	1	100.00		1	100.00		13	100.00		13	100.00	
$\varphi_{\text{CMA}}^{\text{generation}}$	0	100.00		0	100.00		0	100.00		0	100.00	
$\varphi_{\text{CMA}}^{\text{step_size}}$	0	100.00		0	100.00		0	100.00		0	100.00	
$\varphi_{\text{CMA}}^{\text{restart}}$	0	100.00		0	100.00		0	100.00		0	100.00	
$\varphi_{\text{CMA}}^{\text{mean_dist}}$	6	70.11		6	56.83		13	63.61		13	54.12	
$\varphi_{\text{CMA}}^{\text{evopath_c_norm}}$	0	100.00		0	100.00		0	100.00		0	100.00	
$\varphi_{\text{CMA}}^{\text{evopath_s_norm}}$	0	100.00		0	100.00		0	100.00		0	100.00	
$\varphi_{\text{CMA}}^{\text{smallik}}$	1	99.75		1	99.96		13	99.75		13	99.96	
$\varphi_{\text{Dis}}^{\text{ratio_mean_02}}$	71	57.69	(2, 5), (3, 10), (3, 20)	71	62.33	(2, 5), (5, 20)	86	57.36	(2, 5), (3, 20)	86	62.16	
$\varphi_{\text{Dis}}^{\text{ratio_median_02}}$	71	65.95	(3, 5)	71	69.28		86	65.41		86	69.60	
$\varphi_{\text{Dis}}^{\text{diff_mean_02}}$	71	47.75		71	99.52		86	48.77		86	99.52	
$\varphi_{\text{Dis}}^{\text{diff_median_02}}$	71	50.21		71	99.44		86	51.44		86	99.45	
$\varphi_{\text{Dis}}^{\text{ratio_mean_05}}$	27	55.22	(5, 20)	27	60.59		42	54.76	(5, 20)	42	60.32	
$\varphi_{\text{Dis}}^{\text{ratio_median_05}}$	27	59.80		27	64.43		42	59.66	(5, 20)	42	64.57	
$\varphi_{\text{Dis}}^{\text{diff_mean_05}}$	27	47.99		27	99.49		42	49.16		42	99.49	
$\varphi_{\text{Dis}}^{\text{diff_median_05}}$	27	51.16		27	99.46		42	52.88		42	99.48	
$\varphi_{\text{Dis}}^{\text{ratio_mean_10}}$	12	54.63	(5, 20)	12	59.33		25	54.06	(5, 20)	25	58.71	
$\varphi_{\text{Dis}}^{\text{ratio_median_10}}$	12	58.29		12	62.38	(2, 3)	25	57.80		25	61.82	
$\varphi_{\text{Dis}}^{\text{diff_mean_10}}$	12	49.70		12	99.52		25	50.88		25	99.52	
$\varphi_{\text{Dis}}^{\text{diff_median_10}}$	12	53.51		12	99.48		25	55.53		25	99.49	
$\varphi_{\text{Dis}}^{\text{ratio_mean_25}}$	6	54.80		6	58.86		15	53.87		15	58.06	
$\varphi_{\text{Dis}}^{\text{ratio_median_25}}$	6	56.21		6	59.74		15	54.91		15	58.26	
$\varphi_{\text{Dis}}^{\text{diff_mean_25}}$	6	53.78		6	99.55		15	55.29		15	99.55	
$\varphi_{\text{Dis}}^{\text{diff_median_25}}$	6	57.40		6	99.49		15	60.24		15	99.50	
$\varphi_{y\text{-D}}^{\text{skewness}}$	6	36.71		—	—	—	—	—	—	—	—	—
$\varphi_{y\text{-D}}^{\text{kurtosis}}$	6	63.06		—	—	—	—	—	—	—	—	—
$\varphi_{y\text{-D}}^{\text{number_of_peaks}}$	6	32.34		—	—	—	—	—	—	—	—	—

Table S4: TSS nearest features from feature sets Φ_{Lvl} , Φ_{MM} , Φ_{Inf} , and Φ_{NBC} (only \mathcal{T} -based and sample set independent, \mathcal{A} -based are identical to TSS full in Table S2). Features are grouped according to their feature sets (separated by horizontal lines). Features with less than 25% of values equal to \bullet and robustness greater than 0.9, are in gray. N_\bullet denotes the lowest measured number of points from which at most 1% of feature calculations resulted in \bullet ($N_\bullet = 0$ for sample set independent φ). The (D_i, D_j) column shows the pairs of feature dimensions for which the two-sided Wilcoxon signed rank test with the Bonferroni-Holm correction does not reject the hypothesis of equality of median feature values, at the family-wise level 0.05 for each individual feature.

	\mathcal{T}		\mathcal{T}^\top		\mathcal{T}_P		\mathcal{T}_P^\top	
	N_\bullet	rob.(%) (D_i, D_j)	N_\bullet	rob.(%) (D_i, D_j)	N_\bullet	rob.(%) (D_i, D_j)	N_\bullet	rob.(%) (D_i, D_j)
$\varphi_{mmce.lda.10}^{Lvl}$	6	39.47	6	39.47	13	53.01	13	53.01
$\varphi_{mmce.qda.10}^{Lvl}$	6	69.30	6	69.88	13	65.30	13	65.91
$\varphi_{mmce.mda.10}^{Lvl}$	6	28.07	6	28.14	13	27.38	13	27.64
$\varphi_{lda.qda.10}^{Lvl}$	6	80.09	6	80.12	18	92.37	18	92.38
$\varphi_{lda.mda.10}^{Lvl}$	6	44.32	6	42.71	13	46.42	13	48.00
$\varphi_{qda.mda.10}^{Lvl}$	6	81.14	6	80.51	13	78.27	13	77.33
$\varphi_{mmce.lda.25}^{Lvl}$	6	32.64	6	32.64	13	54.19	13	54.19
$\varphi_{mmce.qda.25}^{Lvl}$	6	62.01	6	62.41	13	56.49	13	56.69
$\varphi_{mmce.mda.25}^{Lvl}$	6	22.86	6	22.63	13	27.03	13	26.99
$\varphi_{lda.qda.25}^{Lvl}$	6	76.25	6	76.29	15	94.13	15	94.12
$\varphi_{lda.mda.25}^{Lvl}$	6	32.07 (3,20)	6	27.68 (3,10), (10,20)	13	22.86	13	20.39
$\varphi_{qda.mda.25}^{Lvl}$	6	77.24	6	77.68	13	63.08	13	63.11
$\varphi_{mmce.lda.50}^{Lvl}$	6	22.40	6	22.39	13	18.46	13	18.46
$\varphi_{mmce.qda.50}^{Lvl}$	6	48.24	6	49.46	13	32.88	13	33.15
$\varphi_{mmce.mda.50}^{Lvl}$	6	20.13	6	19.60	13	38.52	13	37.58
$\varphi_{lda.qda.50}^{Lvl}$	6	69.22 (10,20)	6	69.24 (10,20)	15	84.45	15	84.41
$\varphi_{lda.mda.50}^{Lvl}$	6	36.05	6	30.90	13	6.80 (5,20)	13	4.51
$\varphi_{qda.mda.50}^{Lvl}$	6	42.65 (3,20)	6	40.68	13	21.96 (5,20)	13	22.47 (3,5), (5,20)
<hr/>								
$\varphi_{lin.simple.adj.r2}^{MM}$	6	19.64	6	19.62	–	–	–	–
$\varphi_{lin.simple.coef.min}^{MM}$	6	51.95	6	85.41	–	–	–	–
$\varphi_{lin.simple.coef.max}^{MM}$	6	29.73	6	77.68	–	–	–	–
$\varphi_{lin.simple.coef.max.by.min}^{MM}$	6	27.78	6	69.78	–	–	–	–
$\varphi_{lin.w.interact.adj.r2}^{MM}$	100	44.77	100	43.89	–	–	–	–
$\varphi_{quad.simple.adj.r2}^{MM}$	6	50.23	6	52.16	–	–	–	–
$\varphi_{quad.simple.cond}^{MM}$	6	46.45	6	95.21	–	–	–	–
$\varphi_{quad.w.interact.adj.r2}^{MM}$	629	82.50	531	77.81	–	–	–	–
<hr/>								
$\varphi_{h.max}^{Inf}$	6	14.46 (3,5)	6	33.83	13	35.74	13	35.42
$\varphi_{eps.s}^{Inf}$	6	6.59	6	34.65	3056	26.05	3196	54.56
$\varphi_{eps.max}^{Inf}$	6	64.93	6	84.99	13	65.17	13	84.18
φ_{no}^{Inf}	6	1.30	6	3.88	–	–	–	–
$\varphi_{eps.ratio}^{Inf}$	6	27.67	6	44.91	–	–	–	–
<hr/>								
$\varphi_{h.std.ratio}^{NBC}$	6	31.11	6	18.27	–	–	–	–
$\varphi_{h.mean.ratio}^{NBC}$	6	38.98	6	32.96	–	–	–	–
$\varphi_{h.cor}^{NBC}$	6	45.94	6	32.39	–	–	–	–
$\varphi_{str.ratio}^{NBC}$	6	55.23	6	50.78	–	–	–	–
$\varphi_{nb.fitness.cor}^{NBC}$	6	77.17	6	77.13	–	–	–	–

Table S5: TSS knn features from feature sets Φ_{Basic} , Φ_{CMA} , Φ_{Dis} , and $\Phi_{\text{y-D}}$ (only \mathcal{T} -based and sample set independent, \mathcal{A} -based are identical to TSS full in Table S1). Features are grouped according to their feature sets (separated by horizontal lines). Features with less than 25% of values equal to \bullet and robustness greater than 0.9, are in gray. N_{\bullet} denotes the lowest measured number of points from which at most 1% of feature calculations resulted in \bullet ($N_{\bullet} = 0$ for sample set independent φ). The (D_i, D_j) column shows the pairs of feature dimensions for which the two-sided Wilcoxon signed rank test with the Bonferroni-Holm correction does not reject the hypothesis of equality of median feature values, at the family-wise level 0.05 for each individual feature.

	\mathcal{T}		\mathcal{T}^{\top}		$\mathcal{T}_{\mathcal{P}}$		$\mathcal{T}_{\mathcal{P}}^{\overline{}}$			
	N_{\bullet}	rob.(%) (D_i, D_j)	N_{\bullet}	rob.(%) (D_i, D_j)	N_{\bullet}	rob.(%) (D_i, D_j)	N_{\bullet}	rob.(%) (D_i, D_j)		
φ_{dim}	0	100.00	0	100.00	0	100.00	0	100.00		
φ_{obs}	1	92.16	1	92.16	13	92.26	13	92.26		
φ_{CMA}	0	100.00	0	100.00	0	100.00	0	100.00		
$\varphi_{\text{generation}}$	0	100.00	0	100.00	0	100.00	0	100.00		
$\varphi_{\text{step.size}}$	0	100.00	0	100.00	0	100.00	0	100.00		
φ_{restart}	0	100.00	0	100.00	0	100.00	0	100.00		
$\varphi_{\text{CMA.mean.dist}}$	6	78.64	6	98.40	13	93.96	13	98.71		
$\varphi_{\text{evopath.c.norm}}$	0	100.00	0	100.00	0	100.00	0	100.00		
$\varphi_{\text{evopath.s.norm}}$	0	100.00	0	100.00	0	100.00	0	100.00		
$\varphi_{\text{CMA.lik}}$	1	98.81	1	99.95	13	98.80	13	99.96		
φ_{Dis}	74	30.53	74	23.95	109	29.18	109	23.33		
$\varphi_{\text{ratio.mean.02}}$	74	34.49	(5, 10)	74	25.97	109	32.08	109	24.94	
$\varphi_{\text{ratio.median.02}}$	74	50.17	74	96.75	109	50.99	109	96.76		
$\varphi_{\text{diff.mean.02}}$	74	49.55	74	95.54	109	50.37	109	95.47		
$\varphi_{\text{diff.median.02}}$	30	28.43	30	21.63	53	26.56	53	21.19		
$\varphi_{\text{ratio.mean.05}}$	30	35.85	30	24.73	(3, 10)	53	31.45	(2, 20)	53	23.58
$\varphi_{\text{ratio.median.05}}$	30	55.94	30	96.80	53	56.94	53	96.85		
$\varphi_{\text{diff.mean.05}}$	30	55.11	30	95.80	53	56.23	53	95.82		
$\varphi_{\text{diff.median.05}}$	15	25.57	(2, 3), (2, 10), (3, 10), (5, 10)	15	19.13	28	24.33	(5, 10)	28	18.97
$\varphi_{\text{ratio.mean.10}}$	15	32.86	15	21.96	28	29.68	28	21.49		
$\varphi_{\text{ratio.median.10}}$	15	58.33	15	96.96	28	59.42	28	97.02		
$\varphi_{\text{diff.mean.10}}$	15	57.49	15	96.09	28	58.85	28	96.16		
$\varphi_{\text{diff.median.10}}$	6	19.39	6	14.96	15	19.01	15	14.16		
$\varphi_{\text{ratio.mean.25}}$	6	23.38	6	15.76	(3, 5)	15	24.08	15	16.25	
$\varphi_{\text{ratio.median.25}}$	6	62.31	6	97.06	15	62.72	15	97.12		
$\varphi_{\text{diff.mean.25}}$	6	61.67	6	96.27	15	62.60	15	96.36		
$\varphi_{\text{y-D.skewness}}$	6	30.49	–	–	–	–	–	–		
$\varphi_{\text{y-D.kurtosis}}$	6	72.61	–	–	–	–	–	–		
$\varphi_{\text{y-D.number.of.peaks}}$	6	26.63	–	–	–	–	–	–		

Table S6: TSS knn features from feature sets Φ_{Lvl} , Φ_{MM} , Φ_{Inf} , and Φ_{NBC} (only \mathcal{T} -based, \mathcal{A} -based are identical to TSS full in Table S2). Features are grouped according to their feature sets (separated by horizontal lines). Features with less than 25% of values equal to \bullet and robustness greater than 0.9, are in gray. N_{\bullet} denotes the lowest measured number of points from which at most 1% of feature calculations resulted in \bullet ($N_{\bullet} = 0$ for sample set independent φ). The (D_i, D_j) column shows the pairs of feature dimensions for which the two-sided Wilcoxon signed rank test with the Bonferroni-Holm correction does not reject the hypothesis of equality of median feature values, at the family-wise level 0.05 for each individual feature.

	\mathcal{T}		\mathcal{T}^{τ}		$\mathcal{T}_{\mathcal{P}}$		$\mathcal{T}_{\mathcal{P}}^{\tau}$			
	N_{\bullet}	rob.(%) (D_i, D_j)	N_{\bullet}	rob.(%) (D_i, D_j)	N_{\bullet}	rob.(%) (D_i, D_j)	N_{\bullet}	rob.(%) (D_i, D_j)		
$\varphi_{mmce_lda.10}$	6	11.39	6	11.39	13	9.63	13	9.93		
$\varphi_{mmce_qda.10}$	6	67.83	6	69.40	13	69.58	13	70.79	(3,5)	
$\varphi_{mmce_mda.10}$	6	21.15	6	20.32	13	19.93	13	19.25		
$\varphi_{lda_qda.10}$	23	67.38	23	67.38	37	70.31	37	70.32		
$\varphi_{lda_mda.10}$	6	15.74	6	13.69	13	22.17	13	20.80		
$\varphi_{qda_mda.10}$	6	57.54	6	56.51	13	55.10	13	55.06		
$\varphi_{mmce_lda.25}$	6	9.73	6	9.63	13	15.42	(3,20)	13	15.65	(3,20)
$\varphi_{mmce_qda.25}$	6	37.27	6	38.00	13	36.70	13	37.25		
$\varphi_{mmce_mda.25}$	6	17.79	6	16.60	13	15.60	13	14.90		
$\varphi_{lda_qda.25}$	6	73.93	(5,10)	6	73.87	(5,10)	18	89.97	18	89.95
$\varphi_{lda_mda.25}$	6	8.97	6	6.33	13	4.46	13	2.95		
$\varphi_{qda_mda.25}$	6	47.47	6	49.72	13	35.90	13	39.50	(2,10), (3,5)	
$\varphi_{mmce_lda.50}$	6	17.46	6	16.62	13	7.86	13	7.88		
$\varphi_{mmce_qda.50}$	6	34.21	6	34.32	13	23.54	13	27.64		
$\varphi_{mmce_mda.50}$	6	24.08	6	20.56	13	20.74	13	19.07	(2,3)	
$\varphi_{lda_qda.50}$	6	41.38	6	41.37	18	73.19	18	73.01		
$\varphi_{lda_mda.50}$	6	26.79	6	32.00	13	2.70	(5,10)	13	2.30	
$\varphi_{qda_mda.50}$	6	17.30	6	24.22	13	5.95	13	7.69	(5,20)	
$\varphi_{mm_lin_simple_adj_r2}$	6	15.67	6	15.63	–	–	–	–	–	
$\varphi_{mm_lin_simple_coef_min}$	6	97.40	6	63.93	–	–	–	–	–	
$\varphi_{mm_lin_simple_coef_max}$	6	98.12	(2,3)	6	87.04	–	–	–	–	
$\varphi_{mm_lin_simple_coef_max_by_min}$	6	34.41	6	45.65	–	–	–	–	–	
$\varphi_{mm_lin_w_interact_adj_r2}$	100	37.50	100	30.25	–	–	–	–	–	
$\varphi_{mm_quad_simple_adj_r2}$	6	41.50	6	37.91	–	–	–	–	–	
$\varphi_{mm_quad_simple_cond}$	6	92.55	6	87.21	–	–	–	–	–	
$\varphi_{mm_quad_w_interact_adj_r2}$	688	69.48	632	60.02	–	–	–	–	–	
$\varphi_{inf_h_max}$	6	1.94	6	1.57	(3,5)	13	31.85	13	38.67	
$\varphi_{inf_eps_s}$	6	38.77	6	3.58	–	–	–	–	–	
$\varphi_{inf_eps_max}$	6	97.84	6	59.04	–	–	–	–	–	
φ_{inf_n0}	6	0.84	6	0.44	–	–	–	–	–	
$\varphi_{inf_eps_ratio}$	6	17.19	6	5.59	–	–	–	–	–	
$\varphi_{nbc_std_ratio}$	6	20.10	6	14.20	–	–	–	–	–	
$\varphi_{nbc_mean_ratio}$	6	36.38	6	30.42	–	–	–	–	–	
φ_{nbc_cor}	6	28.49	6	26.50	–	–	–	–	–	
$\varphi_{nbc_t_ratio}$	6	41.24	6	26.53	–	–	–	–	–	
$\varphi_{nbc_fitness_cor}$	6	45.12	6	45.14	–	–	–	–	–	

4 Connection of Landscape Features and Model Error Results

We have tested the statistical significance of the MSE and RDE differences for 19 surrogate model settings using TSS full and TSS nearest methods and also the lmm surrogate model utilizing TSS knn, i. e., 39 different combinations of model settings ψ and TSS methods (ψ , TSS), on all available sample sets using the non-parametric two-sided Wilcoxon signed rank test with the Holm correction for the family-wise error. To better illustrate the differences between individual settings, we also count the percentage of cases at which one setting had the error lower than the other. The pairwise score and the statistical significance of the pairwise differences are summarized in Tables S7 and S8.

To compare the convenience of individual features as descriptors of areas where the surrogate model \mathcal{M} with a particular (ψ , TSS) combination has the best performance, we use the Kolmogorov-Smirnov test (KS test) testing the equality of the distribution of values of individual features calculated on the whole testing dataset and on only those sample sets from the testing dataset for which the (ψ , TSS) combination leads to the lowest error (MSE or RDE) among all tested combinations. The hypothesis of distribution equality is tested at the family-wise significance level $\alpha = 0.05$ after the Holm correction. The resulting p-values are summarized in Tables S9–S13.

Table S8: A pairwise comparison of the model settings RDE in different TSS. The percentage of wins of i -th model setting against j -th model setting over all available data is given in the i -th row and j -th column. The numbers in bold mark the row model setting being significantly better than the column model setting according to the two-sided Wilcoxon signed rank test with the Holm correction at family-wise significance level $\alpha = 0.05$.

RDE	TSS	model	full										nearest																								
			GP					SE-Q	SE	CART	CART	OCL	PAIR	PAIR	RDE	RDE	SE	SE-Q	CART	CART	OCL	PAIR	PAIR	RDE	RDE												
			LN	Mat	NN	Q	LN																			Mat	NN	Q									
			win	lose	tie	lose	win																			lose	tie	lose									
GP	Q																																				
full	RF	PAIR	33	66	48	39	35	32	33	35	45	43	54	35	43	34	48	49	27	60	39	31	26	20	21	37	37	33	43	37	33	43	37	33	43		
		SE-Q	52	73	66	58	49	43	43	38	35	36	38	48	55	53	58	59	40	48	41	51	30	61	61	42	34	29	20	21	21	44	44	38	48	43	49
full	lq	PAIR	33	66	48	39	35	32	33	35	45	43	54	35	43	34	48	49	27	60	39	31	26	20	21	37	37	33	43	37	33	43	37	33	43	37	33
		SE-Q	52	73	66	58	49	43	43	38	35	36	38	48	55	53	58	59	40	48	41	51	30	61	61	42	34	29	20	21	21	44	44	38	48	43	49
nearest	RF	PAIR	33	66	48	39	35	32	33	35	45	43	54	35	43	34	48	49	27	60	39	31	26	20	21	37	37	33	43	37	33	43	37	33	43	37	33
		SE-Q	52	73	66	58	49	43	43	38	35	36	38	48	55	53	58	59	40	48	41	51	30	61	61	42	34	29	20	21	21	44	44	38	48	43	49
nearest	lq	PAIR	33	66	48	39	35	32	33	35	45	43	54	35	43	34	48	49	27	60	39	31	26	20	21	37	37	33	43	37	33	43	37	33	43	37	33
		SE-Q	52	73	66	58	49	43	43	38	35	36	38	48	55	53	58	59	40	48	41	51	30	61	61	42	34	29	20	21	21	44	44	38	48	43	49
full	lq	PAIR	33	66	48	39	35	32	33	35	45	43	54	35	43	34	48	49	27	60	39	31	26	20	21	37	37	33	43	37	33	43	37	33	43	37	33
		SE-Q	52	73	66	58	49	43	43	38	35	36	38	48	55	53	58	59	40	48	41	51	30	61	61	42	34	29	20	21	21	44	44	38	48	43	49
nearest	lq	PAIR	33	66	48	39	35	32	33	35	45	43	54	35	43	34	48	49	27	60	39	31	26	20	21	37	37	33	43	37	33	43	37	33	43	37	33
		SE-Q	52	73	66	58	49	43	43	38	35	36	38	48	55	53	58	59	40	48	41	51	30	61	61	42	34	29	20	21	21	44	44	38	48	43	49

Table S9: The p-values of the Kolmogorov-Smirnov (KS) test comparing the equality of probability distributions of individual TSS full feature representatives on all data and on those data on which a particular model setting scored best in MSE. The p-values are after the Holm correction and they are shown only if the KS test rejects the equality of both distributions at the family-wise significance level $\alpha = 0.05$, non-rejecting the equality hypothesis is indicated with —. Zeros indicate p-values below the smallest double precision number.

\mathcal{M}	GP							RF							lmm		lq		
	Gibbs	LIN	Mat	NN	Q	RQ	SE+Q	SECART	CART	OC1	PAIR	PAIR	SCRT	SCRT	SUPP	SUPP	lmm	lq	
settings								MSE	RDE		MSE	RDE	MSE	RDE	MSE	RDE			
φ_{dim}	2e-101	—	3.2e-21	1.3e-3	2.9e-5	1.7e-23	2.8e-13	—	1.3e-59	1.9e-16	—	2.4e-2	3.9e-2	1.5e-3	1.0e-16	7.4e-3	4e-115	7.8e-46	
$\varphi_{\text{obs}}(\mathcal{A})$	1.8e-40	—	1.0e-7	1.7e-7	7.0e-29	5.9e-36	1.6e-21	—	2.6e-43	1.7e-7	8.4e-11	—	2.3e-10	1.1e-6	6.0e-15	1.4e-10	—	3.2e-14	3e-259
$\varphi_{\text{evopath,c, norm}}$	3.5e-7	3.5e-8	7.9e-37	—	2.6e-69	7.6e-62	9.1e-30	2.1e-10	9.9e-20	3.7e-18	4.5e-4	—	1.2e-8	9.3e-8	7.0e-18	2.2e-24	4.3e-24	1e-216	5e-307
$\varphi_{\text{evopath,s, norm}}$	1.3e-88	2.1e-3	9.7e-10	1.5e-25	3.3e-48	6.0e-33	9.2e-17	7.4e-15	5.1e-18	7.0e-13	6.9e-14	2.7e-6	2.6e-5	3.9e-5	1.3e-10	2.1e-14	6.3e-11	1.3e-16	1.1e-13
φ_{restart}	7e-105	1.5e-7	9.7e-20	2.3e-61	7e-273	5e-193	3e-137	3.5e-46	3.3e-21	8.2e-18	1.7e-60	—	2.0e-4	4.1e-9	8.7e-98	5.5e-14	5.1e-37	1.9e-12	2.2e-15
$\varphi_{\text{step.size}}$	0	5.2e-19	1.5e-62	2e-123	1e-267	9e-183	6.1e-90	5.4e-79	5.0e-53	1.5e-57	1.1e-58	2.0e-20	3.4e-48	2.2e-47	2.5e-79	5.6e-46	8.4e-85	1.3e-28	9e-194
$\varphi_{\text{cma.lik}}(\mathcal{A}_{\mathcal{P}}^{\top})$	1.5e-37	1.8e-2	8.2e-7	2.7e-14	2.9e-30	2.8e-33	3.8e-8	6.6e-14	1.7e-9	7.8e-9	4.3e-8	2.0e-3	2.2e-6	1.6e-5	9.3e-14	9.7e-8	4.5e-12	6.0e-34	1.5e-22
$\varphi_{\text{diff.median.02}}(\mathcal{A}^{\top})$	0	2.7e-30	3e-103	3e-159	0	0	4e-160	2e-112	3.9e-94	7e-110	1.1e-91	6.1e-7	8.3e-50	2.3e-38	3.8e-89	5.9e-62	6e-107	3e-103	6e-250
$\varphi_{\text{diff.median.10}}(\mathcal{A}^{\top})$	0	1.9e-35	1e-126	9e-173	0	0	3e-166	2e-130	2.8e-89	4e-118	5.0e-93	4.7e-11	1.8e-62	5.6e-53	2.4e-90	1.4e-61	4e-125	2.5e-82	0
$\varphi_{\text{diff.mean.05}}(\mathcal{A}_{\mathcal{P}}^{\top})$	0	1.6e-35	5e-132	7e-188	0	0	1e-185	7e-138	6e-115	2e-133	1e-104	3.1e-9	3.0e-68	5.8e-55	7e-102	6.5e-81	5e-129	2.0e-81	0
$\varphi_{\text{diff.mean.25}}(\mathcal{A}_{\mathcal{P}}^{\top})$	0	6.2e-40	3e-157	6e-186	0	0	2e-181	4e-142	3e-102	8e-130	7e-102	3.9e-10	4.9e-77	7.2e-60	1.1e-99	1.7e-79	1e-128	1e-103	0
$\varphi_{\text{lvl.lda.qda.10}}(\mathcal{A}_{\mathcal{P}})$	9.7e-29	1.7e-5	8.2e-18	3.4e-19	1.6e-22	4.4e-5	7.8e-25	1.5e-4	5.4e-4	5.4e-12	1.7e-10	—	1.0e-11	1.1e-7	1.7e-35	2.5e-3	1.7e-9	2.0e-56	0
$\varphi_{\text{lvl.lda.qda.25}}(\mathcal{A}_{\mathcal{P}})$	6.9e-30	5.7e-33	6.2e-31	6.1e-8	3.8e-9	1.2e-12	2.6e-16	2.0e-29	7.2e-14	1.2e-23	3.1e-13	1.5e-6	1.6e-44	9.8e-33	3.9e-27	1.3e-14	1.2e-17	3.8e-14	3e-181
$\varphi_{\text{MM}}^{\text{quad.simple.cond}}(\mathcal{A}^{\top})$	7.6e-83	1.4e-9	3.5e-25	8.7e-13	2e-145	1.7e-96	2.9e-46	2.3e-34	8.3e-11	1.1e-11	3.9e-16	—	5.2e-5	5.5e-3	7.3e-8	3.0e-7	1.9e-13	7e-235	1e-127

Table S10: The p-values of the Kolmogorov-Smirnov (KS) test comparing the equality of probability distributions of individual TSS full feature representatives on all data and on those data on which a particular model setting scored best in RDE. The p-values are after the Holm correction and they are shown only if the KS test rejects the equality of both distributions at the family-wise significance level $\alpha = 0.05$, non-rejecting the equality hypothesis is indicated with —. Zeros indicate p-values below the smallest double precision number.

\mathcal{M}	GP								RF								lmm lq		
	Gibbs	LIN	Mat	NN	Q	RQ	SE+Q	—	SECART	CART	OC1	PAIR	PAIR	SCRT	SCRT	SUPP	SUPP	—	—
settings									MSE	RDE		MSE	RDE	MSE	RDE	MSE	RDE		
φ_{dim}	6e-112	3e-182	4.8e-30	4.8e-18	3.0e-14	1.6e-25	2.5e-14	2.2e-8	—	2.8e-12	1.2e-10	1.1e-17	1.1e-26	1.9e-15	1.5e-22	6.6e-5	1.3e-25	1.5e-17	4.1e-72
$\varphi_{\text{obs}}(\mathcal{A})$	2e-286	2e-152	6e-308	5e-103	3e-232	4e-111	8e-179	7e-179	1.5e-17	2.5e-8	1.9e-2	1.4e-4	6.1e-26	4.0e-20	6.4e-5	5.5e-5	7.1e-6	4e-120	4e-280
$\varphi_{\text{evopath.c.norm}}^{\text{CMA}}$	2.6e-56	0	0	3e-131	6e-295	7e-152	1e-170	7e-140	6.9e-4	9.5e-6	2.2e-3	1.2e-4	—	—	3.9e-6	1.4e-7	1.1e-3	1e-172	8e-309
$\varphi_{\text{evopath.s.norm}}^{\text{CMA}}$	5.6e-69	8.8e-27	5.5e-4	3.1e-62	9.8e-13	6.1e-25	3.7e-16	9.0e-20	4.3e-11	7.3e-4	3.9e-2	—	1.4e-11	1.7e-5	1.3e-8	9.6e-4	3.3e-7	4.9e-27	1.7e-21
$\varphi_{\text{restart}}^{\text{CMA}}$	4.3e-2	2.2e-77	1.7e-59	3.5e-6	3.1e-9	1.5e-7	2.2e-25	6.6e-37	5.1e-31	1.1e-4	3.8e-2	—	2.0e-2	—	3.3e-8	1.0e-4	—	1.7e-54	7e-138
$\varphi_{\text{step.size}}^{\text{CMA}}$	0	3e-234	1e-227	0	0	0	0	0	5.3e-75	2.3e-23	1.8e-4	5.5e-6	1.3e-68	2.7e-48	2.4e-23	5.0e-40	3.3e-17	8.7e-36	4.7e-87
$\varphi_{\text{cma.lik}}^{\text{CMA}}(\mathcal{A}^T)$	6.3e-65	9.4e-19	1.3e-53	1.4e-36	2.1e-74	1.3e-48	1.3e-46	5.4e-38	—	—	—	—	7.8e-4	5.3e-3	4.2e-4	4.5e-2	5.8e-9	2.1e-46	5.1e-42
$\varphi_{\text{diff.median.02}}^{\text{Dis}}(\mathcal{A}^T)$	0	9e-234	0	0	0	0	0	0	1.2e-88	1.7e-23	1.0e-7	—	2.7e-72	7.0e-57	9.6e-15	1.8e-37	3.3e-15	2e-104	5e-110
$\varphi_{\text{diff.median.10}}^{\text{Dis}}(\mathcal{A}^T)$	0	0	0	0	0	0	0	0	4.8e-88	3.6e-21	1.3e-9	7.6e-6	1.0e-93	3.3e-79	1.8e-13	1.1e-43	1.6e-12	3.8e-76	1e-130
$\varphi_{\text{diff.mean.05}}^{\text{Dis}}(\mathcal{A}^T)$	0	0	0	0	0	0	0	0	5.2e-98	4.2e-22	1.2e-9	8.6e-4	1.9e-93	4.7e-71	1.7e-8	3.6e-47	1.1e-8	2.9e-66	1e-128
$\varphi_{\text{diff.mean.25}}^{\text{Dis}}(\mathcal{A}^T)$	0	0	0	0	0	0	0	0	1.3e-93	1.3e-20	5.5e-11	6.1e-4	2e-103	2.8e-86	5.5e-9	2.0e-44	3.6e-8	1e-106	5e-201
$\varphi_{\text{lda.qda.10}}^{\text{Lvl}}(\mathcal{A}_{\mathcal{P}})$	6e-221	1e-268	0	1e-105	0	4e-167	2e-241	8e-223	6.8e-6	5.2e-4	1.7e-2	1.2e-7	3.5e-5	2.5e-9	5.1e-4	1.7e-2	—	4e-129	0
$\varphi_{\text{lda.qda.25}}^{\text{Lvl}}(\mathcal{A}_{\mathcal{P}})$	1.6e-54	2.0e-40	3.4e-90	7.7e-24	1.3e-74	1.4e-35	6.3e-45	1.0e-51	5.2e-5	1.2e-3	5.2e-10	1.8e-18	3.0e-36	5.1e-33	3.3e-3	7.5e-5	1.1e-7	5.5e-25	4.8e-53
$\varphi_{\text{quad.simple.cond}}^{\text{MM}}(\mathcal{A}^T)$	1e-190	8.5e-68	6e-220	2.1e-64	0	2e-177	3e-180	4e-148	7.1e-5	1.6e-3	—	8.8e-3	4.3e-9	6.0e-6	2.6e-4	2.0e-3	3.5e-2	0	0

Table S11: The p-values of the Kolmogorov-Smirnov (KS) test comparing the equality of probability distributions of individual TSS nearest feature representatives on all data and on those data on which a particular model setting scored best in MSE. The p-values are after the Holm correction and they are shown only if the KS test rejects the equality of both distributions at the family-wise significance level $\alpha = 0.05$, non-rejecting the equality hypothesis is indicated with —. Zeros indicate p-values below the smallest double precision number.

\mathcal{M}	GP						RF						lmm		lq		
	Gibbs	LIN	Mat	NN	Q	RQ SE+Q	SECART	CART	OC1	PAIR	PAIR	SCRT	SCRT	SUPP	SUPP	—	—
settings							MSE	RDE		MSE	RDE	MSE	RDE	MSE	RDE		
φ_{dim}	0	1.9e-7	8.2e-19	3.8e-3	1.8e-9	5.5e-81	7.9e-3	9.7e-30	5.7e-14	2.9e-3	7.2e-3	2.9e-10	4.4e-7	2.5e-13	1.5e-2	6.7e-36	1.5e-77
$\varphi_{\text{obs}}(\mathcal{T})$	0	5.0e-3	6.1e-6	6.0e-20	6.2e-6	2.2e-9	3.7e-50	1.5e-6	4.5e-35	4.7e-22	2.1e-9	2.0e-5	8.2e-13	2.2e-6	2.3e-24	9.3e-3	3.4e-11
$\varphi_{\text{evopath.c.norm}}^{\text{CMA}}$	5e-131	6.1e-5	1.9e-46	1.1e-7	7.0e-32	5.2e-18	1.6e-33	1.5e-80	3.5e-26	7.9e-19	3.8e-23	5.5e-19	2.7e-17	2.2e-19	7.4e-19	4.7e-30	9.2e-13
$\varphi_{\text{evopath.s.norm}}^{\text{CMA}}$	3.2e-25	2.1e-2	1.7e-3	7.9e-10	2.8e-4	2.5e-20	6.2e-21	1.0e-4	3.2e-9	1.1e-5	2.9e-7	1.4e-5	1.6e-7	8.8e-7	1.6e-6	4.6e-6	3.9e-5
$\varphi_{\text{restart}}^{\text{CMA}}$	2.4e-69	2.5e-4	—	1.7e-2	1.2e-3	2.3e-75	3.8e-42	1.0e-45	2.6e-2	—	3.2e-2	—	3.3e-2	—	7.9e-4	2.5e-4	1.1e-42
$\varphi_{\text{step.size}}^{\text{CMA}}$	8e-311	2.5e-5	2.4e-21	1.3e-4	1.6e-27	0	0	6e-178	6.3e-13	1.6e-14	6.6e-29	3.1e-8	2.1e-16	1.9e-9	9.7e-25	1.7e-34	6.3e-29
$\varphi_{\text{cma.liik}}^{\text{CMA}}(\mathcal{A}_{\mathcal{P}}^{\text{T}})$	8.2e-60	—	6.1e-9	2.0e-4	1.1e-28	3e-182	1e-202	6e-180	1.0e-6	1.2e-4	1.2e-15	2.6e-7	1.9e-5	1.1e-6	1.4e-11	1.6e-10	2.8e-83
$\varphi_{\text{diff.median.10}}^{\text{Dis}}(\mathcal{A}_{\mathcal{P}}^{\text{T}})$	3e-146	1.9e-10	4.9e-37	7.4e-16	5.2e-57	0	0	3.8e-23	1.6e-22	3.8e-38	4.6e-18	5.0e-26	7.3e-23	1.3e-32	1.5e-60	5.9e-45	2.7e-0
$\varphi_{\text{diff.mean.05}}^{\text{Dis}}(\mathcal{A}_{\mathcal{P}}^{\text{T}})$	5e-192	2.4e-10	4.3e-38	4.6e-15	1e-100	0	0	6.3e-34	1.6e-25	9.3e-52	9.9e-27	5.7e-31	5.8e-35	5.2e-43	1.7e-73	2.2e-51	2.3e-0
$\varphi_{\text{diff.mean.25}}^{\text{Dis}}(\mathcal{A}_{\mathcal{P}}^{\text{T}})$	4e-197	3.7e-11	6.3e-47	5.8e-18	8e-101	0	0	5.8e-31	2.3e-25	5.2e-50	9.3e-26	2.0e-30	5.4e-35	1.3e-40	1.0e-79	8.4e-50	9.6e-0
$\varphi_{\text{diff.median.02}}^{\text{Dis}}(\mathcal{T}^{\text{T}})$	1.2e-26	1.9e-14	5.6e-7	2.0e-33	4.8e-21	2e-208	7e-228	3e-106	—	6.3e-5	2.5e-3	—	1.6e-4	—	5.0e-9	2.7e-81	
$\varphi_{\text{lda.qda.10}}^{\text{Lvl}}(\mathcal{A}_{\mathcal{P}})$	4.1e-35	2.2e-2	3.8e-16	1.4e-20	—	2.4e-76	8e-143	6.8e-66	1.8e-4	1.3e-5	3.9e-5	2.0e-7	3.4e-5	2.5e-6	2.1e-14	6.2e-4	1.3e-21
$\varphi_{\text{lda.qda.25}}^{\text{Lvl}}(\mathcal{T}_{\mathcal{P}})$	9.5e-15	3.2e-11	—	8.0e-14	2.9e-5	1.4e-15	5.7e-23	2.7e-22	1.1e-4	2.6e-5	6.1e-15	8.9e-15	1.6e-4	2.4e-12	9.7e-13	4.5e-16	3.7e-12
$\varphi_{\text{quad.simple.cond}}^{\text{MM}}(\mathcal{T}^{\text{T}})$	8.8e-96	—	6.8e-6	1.9e-10	3.3e-38	4e-111	2e-118	3.0e-90	2.2e-11	1.7e-8	5.2e-8	5.6e-4	2.7e-9	7.4e-3	9.1e-8	1.3e-4	4.4e-5

Table S12: The p-values of the Kolmogorov-Smirnov (KS) test comparing the equality of probability distributions of individual TSS nearest feature representatives on all data and on those data on which a particular model setting scored best in RDE. The p-values are after the Holm correction and they are shown only if the KS test rejects the equality of both distributions at the family-wise significance level $\alpha = 0.05$, non-rejecting the equality hypothesis is indicated with —. Zeros indicate p-values below the smallest double precision number.

\mathcal{M}	GP							RF							lmm		lq		
	Gibbs	LIN	Mat	NN	Q	RQ	SE+Q	SECART	CART	OC1	PAIR	PAIR	SCRT	SCRT	SUPP	SUPP	lmm	lq	
settings								MSE	RDE		MSE	RDE	MSE	RDE	MSE	RDE			
φ_{dim}	0	2e-189	1.2e-31	1.5e-28	9.2e-32	2.6e-15	7.0e-10	5.6e-44	9.5e-7	2.3e-10	2.2e-34	2.4e-26	8.3e-11	1.5e-24	1.4e-8	4.3e-59	2.0e-29	7.8e-54	2.7e-7
$\varphi_{\text{obs}}(\mathcal{T})$	0	9.3e-50	1.2e-11	4.7e-16	7.0e-54	1.7e-15	1.5e-12	3.1e-48	2.1e-5	8.1e-5	7.5e-20	4.4e-16	7.3e-5	5.3e-16	9.8e-5	6.6e-37	1.0e-15	4.8e-58	1.2e-28
$\varphi_{\text{evopath.c.norm}}^{\text{CMA}}$	2e-171	0	0	1e-132	6.0e-83	5e-159	4e-202	2e-284	3.3e-2	3.3e-2	2.2e-5	—	3.4e-2	1.5e-2	1.9e-3	4.2e-12	4.9e-5	3e-202	4.5e-13
$\varphi_{\text{evopath.s.norm}}^{\text{CMA}}$	1.0e-67	6.7e-34	1.0e-17	2.6e-45	4.1e-12	1.1e-9	5.8e-17	7.7e-10	5.3e-3	2.7e-3	1.4e-3	1.3e-3	2.1e-2	6.0e-6	—	7.3e-5	1.5e-4	2.2e-71	1.5e-59
$\varphi_{\text{restart}}^{\text{CMA}}$	4.0e-93	2.9e-91	1.9e-83	7.1e-43	1e-146	2e-280	0	2e-322	1.1e-2	—	1.6e-3	3.2e-4	3.5e-4	1.9e-4	4.4e-2	5.7e-7	3.4e-2	2e-196	3e-270
$\varphi_{\text{step.size}}^{\text{CMA}}$	0	1e-236	0	2e-285	7e-234	8.6e-80	3e-139	2.8e-72	1.0e-22	5.3e-22	1.7e-19	3.5e-20	2.5e-17	9.8e-27	2.5e-16	3.9e-20	1.6e-20	2e-191	9e-138
$\varphi_{\text{cma.lik}}^{\text{CMA}}(\mathcal{A}_{\mathcal{P}}^{\text{T}})$	6.9e-64	2.1e-14	1.4e-50	2.5e-31	2.5e-86	6.3e-71	5.2e-95	1.3e-86	4.3e-8	1.9e-8	9.0e-11	6.4e-11	7.3e-13	1.0e-9	2.0e-11	3.4e-7	5.2e-72	3.4e-12	
$\varphi_{\text{diff.median.10}}^{\text{Dis}}(\mathcal{A}_{\mathcal{P}}^{\text{T}})$	1e-214	0	0	0	3e-307	0	0	0	1.2e-23	4.5e-24	1.5e-15	3.9e-27	1.2e-15	5.9e-28	3.8e-16	1.5e-15	4.6e-16	0	5e-225
$\varphi_{\text{diff.mean.05}}^{\text{Dis}}(\mathcal{A}_{\mathcal{P}}^{\text{T}})$	1e-191	0	0	0	0	0	0	0	2.6e-22	8.3e-21	9.9e-20	1.6e-29	3.8e-15	1.9e-29	3.8e-19	9.5e-15	4.9e-14	0	0
$\varphi_{\text{diff.mean.25}}^{\text{Dis}}(\mathcal{A}_{\mathcal{P}}^{\text{T}})$	6e-197	0	0	0	0	0	0	0	2.6e-22	2.7e-21	1.7e-20	1.3e-30	9.8e-15	9.5e-31	3.6e-19	2.7e-15	5.0e-14	0	2e-317
$\varphi_{\text{diff.median.02}}^{\text{Dis}}(\mathcal{T}^{\text{T}})$	1.0e-22	8e-132	9.6e-62	2.9e-84	1e-107	5e-262	0	4e-256	—	1.3e-3	—	1.2e-3	1.1e-3	5.3e-3	1.7e-2	3.4e-5	9.7e-6	6e-200	1e-215
$\varphi_{\text{lda.qda.10}}^{\text{Lvl}}(\mathcal{A}_{\mathcal{P}})$	8.2e-52	3e-266	0	2e-116	9e-130	2.1e-26	1.4e-19	6.8e-31	7.1e-3	2.4e-5	3.5e-3	1.7e-5	8.8e-6	2.8e-4	—	1.7e-3	1.3e-2	1.8e-49	5e-107
$\varphi_{\text{lda.qda.25}}^{\text{Lvl}}(\mathcal{T}_{\mathcal{P}})$	6.8e-88	8.2e-12	1.0e-22	2.3e-17	1.2e-42	2e-268	9e-231	1e-186	4.0e-6	1.4e-3	5.1e-7	1.3e-10	6.1e-5	7.5e-10	2.7e-9	2.2e-11	2.5e-8	7e-146	8.2e-85
$\varphi_{\text{quad.simple.cond}}^{\text{MM}}(\mathcal{T}^{\text{T}})$	3.4e-30	3.9e-71	4.2e-27	1.7e-22	3.3e-58	1.1e-46	9.8e-55	4.2e-55	2.4e-4	6.2e-4	—	1.2e-3	3.5e-3	6.8e-4	—	—	—	1.1e-21	6.0e-16

Table S13: The p-values of the Kolmogorov-Smirnov (KS) test comparing the equality of probability distributions of individual TSS knn feature representatives on all data and on those data on which the Imm model setting scored best in MSE and RDE. The p-values are after the Holm correction and they are shown only if the KS test rejects the equality of both distributions at the family-wise significance level $\alpha = 0.05$. Zeros indicate p-values below the smallest double precision number.

	φ_{dim}	$\varphi_{\text{obs}}(\mathcal{A}_P)$	$\varphi_{\text{evopath.s.norm}}^{\text{CMA}}$	$\varphi_{\text{restart}}^{\text{CMA}}$	$\varphi_{\text{cma.lik}}^{\text{CMA}}(\mathcal{A}_P^T)$	$\varphi_{\text{cma.lik}}^{\text{CMA}}(\mathcal{T}_P)$	$\varphi_{\text{diff.mean.10}}^{\text{Dis}}(\mathcal{A}^T)$	$\varphi_{\text{diff.median.02}}^{\text{Dis}}(\mathcal{A}^T)$	$\varphi_{\text{diff.mean.10}}^{\text{Dis}}(\mathcal{T}_P^T)$	$\varphi_{\text{diff.mean.05}}^{\text{Dis}}(\mathcal{T}^T)$	$\varphi_{\text{eps.max}}^{\text{Inf}}(\mathcal{T})$	$\varphi_{\text{lda.qda.10}}^{\text{Lvl}}(\mathcal{A}_P)$	$\varphi_{\text{lda.qda.25}}^{\text{Lvl}}(\mathcal{A}_P)$	$\varphi_{\text{quad.sample.cond}}^{\text{MM}}(\mathcal{T})$
MSE	5.2e-32	9.2e-08	1.6e-63	1.9e-75	1.2e-78	3e-267	0	0	8.3e-126	7.4e-161	0	1.1e-23	2.8e-60	2e-25
RDE	9.5e-45	1.2e-28	2.8e-67	1.4e-196	1.6e-46	0	0	0	2.8e-188	4.9e-209	0	9.2e-14	7.4e-119	6.6e-319

References

- Bajer, L., Pitra, Z., Repický, J., and Holeňa, M. (2019). Gaussian process surrogate models for the CMA Evolution Strategy. *Evolutionary Computation*, 27(4):665–697.
- Hansen, N. (2006). The CMA evolution strategy: A comparing review. In *Towards a New Evolutionary Computation*, Studies in Fuzziness and Soft Comp., pages 75–102. Springer.
- Hansen, N., Auger, A., Mersmann, O., Tusa, T., and Brockhoff, D. (2016). COCO: A platform for comparing continuous optimizers in a black-box setting. arXiv:1603.08785.
- Hansen, N. and Ostermeier, A. (1996). Adapting arbitrary normal mutation distributions in evolution strategies: The covariance matrix adaptation. CEC '96., pages 312–317. IEEE.
- Kern, S., Hansen, N., and Koumoutsakos, P. (2006). Local Meta-models for Optimization Using Evolution Strategies. PPSN '06, pages 939–948. Springer.
- Kerschke, P. (2017a). *Automated and Feature-Based Problem Characterization and Algorithm Selection Through Machine Learning*. Dissertation, University of Münster. Publication status: Published.
- Kerschke, P. (2017b). Comprehensive feature-based landscape analysis of continuous and constrained optimization problems using the R-package flacco. *ArXiv e-prints*.
- Kerschke, P. and Dagefoerde, J. (2017). *flacco: Feature-Based Landscape Analysis of Continuous and Constraint Optimization Problems*. R-package v. 1.7.
- Kerschke, P., Preuss, M., Wessing, S., and Trautmann, H. (2015). Detecting funnel structures by means of exploratory landscape analysis. GECCO '15, pages 265–272.
- Lunacek, M. and Whitley, D. (2006). The dispersion metric and the CMA evolution strategy. GECCO '06, pages 477–484.
- Mersmann, O., Bischl, B., Trautmann, H., Preuss, M., Weihs, C., and Rudolph, G. (2011). Exploratory landscape analysis. GECCO '11, pages 829–836.
- Muñoz, M. A., Kirley, M., and Halgamuge, S. K. (2015). Exploratory landscape analysis of continuous space optimization problems using information content. *IEEE Transactions on Evolutionary Computation*, 19(1):74–87.
- Pitra, Z., Bajer, L., and Holeňa, M. (2016). Doubly trained evolution control for the Surrogate CMA-ES. PPSN '16, pages 59–68. Springer.
- Pitra, Z., Koza, J., Tumpach, J., and Holeňa, M. (2022). Landscape analysis for surrogate models in the evolutionary black-box context. arXiv, 2203.11315:1–34. Under review in journal.
- Pitra, Z., Repický, J., and Holeňa, M. (2019). Landscape analysis of Gaussian process surrogates for the covariance matrix adaptation evolution strategy. GECCO '19, pages 691–699.